NACA RM E57A21

NACA

RESEARCH MEMORANDUM

INVESTIGATION OF A HIGH-PERFORMANCE TOP INLET TO MACH NUMBER OF 2.0 AND AT ANGLES OF ATTACK TO 20°

By Donald J. Vargo, Philip N. Parks, and Owen H. Davis

Lewis Flight Propulsion Laboratory
Cleveland, Ohio

NATIONAL ADVISORY COMMITTEE
FOR AERONAUTICS

WASHINGTON

March 20, 1957
Declassified October 28, 1960

TABLE OF CONTENTS

NATIONAL ADVISORY COMMITTEE FOR AERONAUTICS

RESEARCH MEMORANDUM

INVESTIGATION OF A HIGH-PERFORMANCE TOP INLET TO MACH NUMBER OF 2.0 AND AT ANGLES OF ATTACK TO 20°

By Donald J. Vargo, Philip N. Parks, and Owen H. Davis

SUMMARY

Several top-inlet configurations were tested on a body of revolution in the 8- by 6-foot supersonic wind tunnel at angles of attack from 0° to 20° and at free-stream Mach numbers of 1.5 to 2.0. The effect on performance of the following variables was studied: throat bleed, ramp perforations, inlet approach surface, side fairings, fuselage fences, canopies, and a simulated 60° delta wing. For comparison, performance was also obtained with the inlet in the bottom location.

For the inlet with side fairings, throat bleed greatly increased pressure recovery and stability while decreasing distortion throughout the angle-of-attack range. Ramp perforations provided slight increases both in inlet pressure recovery and stability and had essentially no effect on distortion.

Two inlet approach surfaces (round and flat) were tested. No difference in inlet performance was detected up to an angle of attack of 9.5°; however, at larger angles of attack up to 20° the round approach gave higher pressure recovery than did the flat approach.

Three fence lengths were tested. With the exception of the short fence they were generally ineffective in improving angle-of-attack performance.

The canopy configurations caused slight reductions of 3 to 5 percent in pressure recovery at low angles of attack from 0° to 5° and a free-stream Mach number of 2.0. At greater angles of attack the configurations with canopies were better than all other inlets tested, obtaining pressure recoveries at Mach 2.0 of 92, 84, and 70 percent at angles of attack of 9.5°, 15°, and 20°, respectively. Pressure distortions for the canopies were generally slightly higher than those for other configurations, with critical values of about 10 percent at a free-stream Mach number of 2.0 and angles of attack from 0° to 20°.

The wings decreased both inlet pressure recovery and stability at angle of attack for both longitudinal positions examined.

INTRODUCTION

Previous work has shown that the angle-of-attack performance of a top inlet is poor (refs. 1 to 4). However, reference 5 points out that top-inlet performance can be made competitive with that in other locations by the use of fuselage fences. Since the top inlet shows promise of improvement, the work of references 4 and 5 has been extended by the investigation reported here. The variables of this test include throat bleed and ramp perforations, side fairings, fuselage fences, faired and unfaired canopies mounted ahead of the inlet, and wings. The investigation was performed with a double-ramp inlet designed to have two oblique shocks meet ahead of the cowl lip at a free-stream Mach number of 2.0. This inlet study was conducted in the 8- by 6-foot supersonic wind tunnel at the NACA Lewis laboratory. Data were obtained at Mach numbers of 1.5, 1.8, and 2.0 and angles of attack from 0° to 20°. The test Reynolds number per foot of test section length was about 5.4×10^6.

SYMBOLS

A_I	inlet capture area
A_C	compressor-face flow area of engine used in analysis, 4.54 sq ft
C_D	model drag coefficient based on maximum cross-sectional area
C_L	model lift coefficient based on maximum cross-sectional area
D	full-scale configuration drag
F	full-scale engine thrust
F_i	ideal engine thrust (based on 100-percent pressure recovery at altitude of 35,000 ft on standard day)
h	height of boundary-layer splitter plate from fuselage, 0.50 in.
M	Mach number
m	mass-flow rate, slugs/sec
P	total pressure
ΔP	$P_{max} - P_{min}$

p	static pressure
Δp	internal static-pressure variation
α	angle of attack
β	flow angle at survey rake
δ	boundary-layer thickness

Subscripts:

av	average
max	maximum
min	minimum
0	free stream
1	inlet
2	diffuser-exit station
3	mass-flow measuring station

APPARATUS AND PROCEDURE

Model

The model of the present investigation is illustrated photographically in figure 1(a) and schematically in figure 1(b). The model was sting-mounted from a tunnel strut with an internal strain-gage balance connecting the model to the sting. The variation of the internal model duct area is shown in figure 2. The mass flow through the duct was varied by a remotely controlled plug which can be seen in figure 1.

Inlet details are shown schematically and photographically in figure 3. Two approach surfaces were tested, the fully rounded body contour and the flat surface, as can be seen in figures 3 and 4. Boundary layer was removed with a wedge-type diverter (mounted under the compression surface) which positioned the compression ramp at a height of 1.35 times the boundary-layer thickness at zero angle of attack. Ramp angles of 10.4° and 11.1° for the first and second ramps were chosen to provide near-optimum two-shock pressure recovery at a free-stream Mach number of 2.0. The design was such that the two oblique shocks fell just outside the lip at this design Mach number. The inlet was tested with and without

side fairings which were designed to minimize side flow spillage ahead of the terminal shock and, hence, provide increased pressure recovery.

The throat bleed system (fig. 3(b)) was adapted to this inlet from previous bleed studies (refs. 6 to 10). Air was bled through a flush slot just downstream of the throat. The slot opening was approximately 42 percent of the inlet throat area. The bleed air was discharged at side ports through interchangeable restrictor plates which controlled the bleed flow rate (see exit hole, fig. 3(b)).

Ramp perforations examined in the test are shown in figures 3(a) and (c). Four perforated ramps were used, three with only the second ramp perforated and the fourth having both ramps perforated. The amount of perforated hole area (fig. 3(a)), designated as a percent of inlet capture area, varied from 3.4 to 9.53 percent.

Three fences, designated as short, medium, and long, were alternately tested on top of the fuselage ahead of the inlet (fig. 3(d)). A photograph of the short fences is shown in figure 3(e). The fences were used as a means of preventing the boundary-layer crossflow on the fuselage from entering the inlet at angle of attack as was done in reference 5.

Figure 4(a) shows a schematic diagram of the wing and the two canopies which were investigated to determine their effects on inlet performance. Photographs of the canopies mounted ahead of the inlet on the round approach surface are presented in figures 4(b) and (c). The canopy shown in figure 4(c) was faired into the fuselage in an attempt to provide a more uniform flow into the inlet.

The stub wing simulated a 60° delta configuration which was cut off at the point beyond which it could no longer influence the inlet. Inlet performance was determined for two longitudinal wing positions as shown in figure 4(a). Figure 4(e) shows the forward installation. Both positions may, however, be too far forward to represent a practical configuration.

Instrumentation

To survey the flow conditions ahead of the inlet a combined rake and instrumented wedge configuration was used (fig. 5(a)). The fuselage flow survey is presented for the flat approach (fig. 5(b)), the flat approach with medium fences (fig. 5(c)), and the unfaired canopy on the round approach surface (fig. 5(d)). Figure 5(e)) presents a summary of the boundary-layer thickness for the flat approach surface and the medium-fence configuration.

The diffuser-exit total pressure was obtained by averaging the 41 area-weighted total-pressure tubes located at station 2 (see fig. 1(b)).

The inlet mass-flow ratio was determined from six wall static taps at station 3 (fig. 1(b)) and by assuming that the exit plug was choked. The drag was computed by excluding from the balance forces the base force and the change in total momentum of the internal flow from the free stream to the mass-flow measuring station. Thrust-minus-drag used in the performance analysis was obtained by using a present-day turbojet engine and a full-scale configuration drag which was modified by the inlet area changes necessary for matching considerations.

Data were obtained at free-stream Mach numbers of 1.5, 1.8, and 2.0 and at angles of attack from 0° to 20°.

RESULTS AND DISCUSSION

Inlet Performance with Bleed

Reference performance (zero bleed). - The performance of the top-mounted inlet with a flat approach surface is presented in figure 6(a). Pressure recovery P_2/P_0, mass flow m_3/m_0, engine-face total-pressure distortion $\Delta P_2/P_2$, and drag coefficient C_D are presented at free-stream Mach numbers of 1.5 to 2.0 and angles of attack from 0° to 9.5°. At a free-stream Mach number of 2.0 and zero angle of attack, a peak pressure recovery of 0.864 and maximum mass-flow ratio of 0.894 were obtained. Critical distortion values varied between 10 to 20 percent for all Mach numbers and all angles tested. Also at Mach 2.0 and zero angle of attack, the stability range was about 0.15 of the critical mass-flow ratio. Instability is arbitrarily defined as a duct internal static-pressure fluctuation greater than 5 percent of the free-stream total pressure P_0.

Figure 6(b) shows the effect of adding side fairings to the inlet of figure 6(a) (top inlet, flat approach). Side fairings were used to eliminate end effects at the edge of the inlet ramp. At a free-stream Mach number of 2.0 and zero angle of attack, a peak pressure recovery of 0.873 and a maximum mass-flow ratio of 0.930 were obtained. Critical distortions were increased to the 20 percent level and stability was decreased slightly. Unless specifically mentioned as being otherwise, all other configurations were tested with inlet side fairings.

With throat bleed. - In an attempt to improve inlet performance in the manner used in references 6 to 10, increasing amounts of throat bleed were tested, and data are shown for various angles of attack in figure 7. The results presented are for pressure recovery, mass flow, compressor-face total-pressure distortion, and drag coefficient (the latter at angles of attack from 0° to 9.5° only).

The arbitrary designations of 2-, 4-, 6-, and 8-percent bleed used in figures 7(a) to (d), respectively, refer to the approximate percent of critical mass flow bled off at a free-stream Mach number of 2.0 and zero angle of attack. The 2-, 4-, and 6-percent bleeds were tested at angles of attack from 0° to 9.5° while the 8-percent bleed was tested at angles of attack from 0° to 20°. With the exception of the 6-percent bleed (fig. 7(c)), the amount of bleed was controlled by changing the bleed exit area. (For the 6-percent bleed condition the center portion of the throat bleed slot was faired over, for which case the mass flow choked at the throat slot rather than the bleed exit.)

Bleed was most effective in increasing pressure recovery for all angles of attack at a Mach number of 2.0 and at angles of attack other than zero at Mach numbers of 1.8 and 1.5. For example, at Mach number 2.0 and zero angle of attack peak pressure recovery was increased from 0.873 for no bleed to 0.952 for 8-percent bleed (comparing figs. 6(b) and 7(d)). Minimum drag was increased by a drag coefficient value of 0.01 for the drag values obtained (0° to 9.5°). Small amounts of bleed to 4 percent caused slight decreases in inlet stability. However, further bleed increases caused large stability gains at angles of attack to 9.5°. At Mach 2.0 and zero angle of attack the inlet with 8-percent bleed was stable down to a mass-flow ratio of 0.158. Increasing throat bleed decreased critical distortion levels from 5 to 10 percent. In the subsequent discussion mention of the basic inlet configuration refers to the 8-percent bleed configuration with side fairings. Also, all other configurations from this point on were tested utilizing the 8-percent throat bleed configuration.

The effect of adding maximum throat bleed (8 percent) to the inlet configuration without side fairings is shown in figure 8 for a free-stream Mach number of 2.0 and angles of attack from 0° to 9.5°. At this Mach number and zero angle of attack peak recovery was increased from 0.864 to 0.915 by the use of this bleed (comparing figs. 6(a) and 8). Thus, it appears that the 8-percent bleed configuration gave about the same improvement in percentage points of pressure recovery whether side fairings were used or not.

Figure 9 shows the effect of angle of attack and Mach number on the diffuser-exit total-pressure contours at critical flow with and without throat bleed. Throat bleed improved the symmetry of the flow except at the highest angle of attack shown (9.5°) and free-stream Mach numbers less than 2.0.

With ramp bleed. - Previous tests have shown that bleeding small amounts of air through ramp perforations can improve pressure recovery and stability (e.g., see refs. 11 to 13). Several ramps with varying amounts of perforated area were included in this study (figs. 3(a) and (c)), and the results are presented in figure 10. With the exception

of the configuration of figure 10(d) which had perforations on both ramps, all perforated area was on the second ramp. It was noticed that with both ramps perforated, high-pressure air from the second ramp bled out through the first-ramp perforations. However, no apparent detrimental effects were noticed which could be attributed to this circulating flow.

In general, both pressure recovery and stability were increased by perforating the ramp surface. Because of an inability to determine the exact amount of flow through perforations, no comparison is made with throat bleed. However, for the inlet tested it is believed that for a given amount of bypassed air, throat bleed produces a greater increase in pressure recovery than do perforations.

Summary of inlet performance with throat bleed. - Figure 11 presents summary plots comparing thrust-minus-drag and critical distortions of the no-bleed and the various bleed configurations at a free-stream Mach number of 2.0 and angles of attack from 0° to 9.5°. Thrust-minus-drag is presented for a given engine at 35,000 feet and standard conditions as a function of inlet size (shown as a ratio of full-scale inlet area to compressor flow area). For all angles of attack 4-percent bleed gave the highest thrust-minus-drag. Figure 11(b) presents the angle-of-attack performance for an inlet sized for maximum thrust-minus-drag at a free-stream Mach number of 2.0 and zero angle of attack. The figure indicates that if the inlet were sized for optimum performance of a given bleed system at zero angle of attack, the 4-percent bleed configuration would maintain its superiority over the angle-of-attack range.

The distortion values at critical flow for the various bleed configurations are presented in figure 11(c). The use of 2-percent throat bleed lowered the no-bleed distortion from a value of approximately 20 percent to slightly less than 10 percent. Further increases in bleed caused very little decrease in critical distortion. Because, with throat bleed, the present inlet is too small to match present-day turbojet engines near critical flow, the diffuser-exit Mach numbers are too low. For this reason the presented distortion values are slightly optimistic. Reference 14 indicates that the distortion values would be 3 to 4 percent greater if the inlet size (and, hence, critical compressor-face Mach number) were increased to match an engine near critical inlet flow.

Inlet Performance with Fences

As previously mentioned, reference 5 showed that fences could be used to control body crossflow and improve inlet performance at angle of attack. The inlet of reference 5 was located 7.5 maximum body diameters from the nose, while in the present program fence effects were studied with an inlet located 5 diameters from the nose of the model. Results in the form of pressure recovery, pressure distortion, and thrust-minus-

drag as functions of mass-flow ratio are presented in figure 12 for the three fence arrangements of figure 3(d). Data are presented at angles of attack from 0° to 9.5° with the exception of the short fences with side fairings which were tested from 0° to 20°. The medium and long fences (figs. 12(c) and (d)) were essentially of no value in improving pressure recovery at angle of attack. At an angle of attack of 9.5° they decreased the recovery below that of the no-fence configuration (fig. 7(d)). The short fence improved the pressure recovery by 2 to 3 percent at all angles of attack of the inlet without side fairings (figs. 12(a) and 8), but the use of side fairings alone (fig. 7(d)) gave comparable performance. The short fence used in conjunction with side fairings (fig. 12(b)) improved pressure recovery only slightly at angles of attack of 5° and 9.5° and had no effect on pressure recovery at the higher angles. Stability with fence configurations was decreased slightly. No large change in drag was apparent. It appears from these results as compared to data of reference 5 that fences lose their attractiveness when used with a basically high-performance inlet (such as one in the present case which employs throat bleed) or when used with inlets located near the body nose. An interesting characteristic of the fence configurations is that when they became unstable, the shock in its forward travel moved out onto the fuselage almost the entire length of the fence. The effect of fences on diffuser-exit total-pressure contours at varying angle of attack is presented in figure 13. In general, the changes in pressure contours due to fence installation were slight.

Comparisons with Bottom Inlet

In order to obtain reference values whereby top-inlet performance could be evaluated in a manner similar to reference 5, the inlet was tested in the bottom location, and the results appear in figure 14. The top inlet, the inlet with short fences, and the bottom inlet are compared in figure 15 on the basis of thrust-minus-drag and lift coefficient. At most Mach numbers and most angles of attack up to 9.5° the basic inlet (inlet with 8-percent bleed and side fairings) was better at a constant lift coefficient than the bottom-inlet location or the top inlet with short fences. The slightly higher pressure recoveries of the short-fence and bottom-inlet configurations at angle of attack were generally offset by the slightly lower drag of the basic configuration. Caution should be exercised in interpreting these thrust-minus-drag results, since the comparison is based on forebody drag alone. Simple theoretical considerations indicate that such a comparison tends to favor the top-inlet location.

Inlet Performance with Round Approach and Canopies

The performance of the top inlet with a round approach surface is presented in figure 16 at angles of attack from 0° to 20°. A comparison

of the round and flat approaches shows that the pressure recoveries are comparable to an angle of attack of 9.5°; however, at greater angles of attack to 20° the round approach becomes superior to the flat approach. The same configuration tested at angles of 15° and 20° is presented in figure 17 with the splitter height reduced from 0.50 to 0.25 inch. No boundary-layer survey was made for the round approach, but if the value of 0.34 inch for the zero-angle-of-attack flat approach is assumed for the boundary-layer thickness δ, the h/δ is reduced to 0.736. This reduction caused no significant variation in pressure recovery, although the duct static pressure in the inlet fluctuated from 5 to 15 percent of free-stream total pressure for almost every point tested.

A canopy was mounted and tested on the round approach surface, and the results are presented in figure 18. The original canopy is designated as the unfaired canopy and was tested at angles of attack from 0° to 20° (fig. 18(a)). At a free-stream Mach number of 2.0 and angles of attack of 9.5°, 15°, and 20°, pressure recoveries of 0.920, 0.843, and 0.698 were obtained; however, at an angle of attack of 0° the peak pressure recovery was 90 percent. This lower recovery at zero angle of attack was attributed to separation occurring off the rear of the canopy (see schlieren photographs, fig. 19). In an effort to reduce this separation and improve recovery at zero angle of attack, the back of the canopy was refaired to form a gentler slope to the body, and the results are presented in figure 18(b). This faired canopy appreciably raised the pressure recovery near critical flow at zero angle of attack, but decreased the pressure recovery at higher angle of attack from that obtained with the unfaired canopy. The unfaired canopy was also studied with side fairings removed from the inlet at angles of attack of 15° and 20°. The data presented in figure 18(c) show appreciable gains in recovery at an angle of attack of 15° over the configuration having side fairings.

Wing Effects on Inlet Performance

A simulated 60° delta wing was tested in two locations designated as the forward and aft positions (fig. 4(a)), and the results are presented in figure 20. It may be noted, however, that the leading-edge location may be conceivably too far forward for a practical configuration. Slight decreases in inlet pressure recovery occurred for the forward wing positions at angles of attack of 5° and 9.5°. These decreases are believed due to expansions occurring around the wing leading edge at angle of attack. Little effect on inlet performance was observed for the wing mounted in the aft position. However, both wing positions caused stability decreases when compared to the basic configuration.

Comparison of Alternate Configurations

Figure 21(a) presents a summary of pressure recoveries at angles of attack from 0° to 20° of the following configurations: (1) the flat approach basic inlet having 8-percent bleed and side fairings in the top and bottom locations, (2) the short-fence configuration, (3) the round approach inlet having 8-percent bleed and side fairings, and (4) the unfaired canopy with and without inlet side fairings (for angles of attack of 15° and 20° only). The data are shown for the diffuser-exit Mach number which represents best thrust-minus-drag at zero angle of attack.

Up to an angle of attack of about 9.5° all the inlets yielded about the same pressure recovery except those in the presence of the canopy. Above an angle of attack of 9° the top inlets with the flat approach decreased abruptly in pressure recovery. The inlets with a round approach, however, were less sensitive in obtaining the highest pressure recoveries. The presence of a canopy above an angle of attack of 9° did not prove detrimental to the performance of the inlet with the round approach. The superiority of the round over the flat approach may result from the somewhat better streamlining of the round approach in the crossflow direction, in addition to the greater boundary-layer scoop height for the round approach in all vertical planes other than the center plane. Also shown on the figure for comparison are unpublished data for a bottom inlet at angles of attack to 20°. The inlet had a 14° ramp with throat bleed and was located 6.2 body diameters aft of the nose on a body of revolution having a flat approach surface. Based on this trend, the bottom inlet of the present study would appear to provide considerably higher recoveries than the other configurations at the high angles of attack.

Perhaps the most important aspect to note is the stability at high angle of attack. It is significant that most configurations were relatively stable over the entire angle-of-attack range tested.

Figure 21(b) presents the pressure distortion values for angles of attack from 0° to 20° corresponding to the data presented in figure 21(a). An examination of the figure indicates that most values are in the range of 3 to 10 percent with maximums occurring at about 9.5° angle of attack. These pressure distortion data may be somewhat optimistic since, as previously mentioned, the diffuser-exit Mach numbers (and, hence, pressure distortion levels) are somewhat low for matching typical engines near the critical flow conditions.

SUMMARY OF RESULTS

A top-inlet model having a two-oblique-shock compression ramp designed for a Mach number of 2.0 was tested in the 8- by 6-foot supersonic wind tunnel at angles of attack from 0° to 20° and free-stream Mach

numbers of 1.5 to 2.0. Variables tested were throat bleed, ramp perforations, inlet side fairings, fences, canopies, and simulated 60° delta wings. For comparison purposes the basic inlet (with side fairings and 8-percent throat bleed) was studied in a bottom location. Results obtained are as follows:

1. Throat bleed (with inlet side fairings) increased pressure recovery from 0.873 (no bleed) to 0.952 (8-percent bleed) at a free-stream Mach number of 2.0 and zero angle of attack. The marked improvements in pressure recovery and thrust-minus-drag at zero angle of attack were maintained over the entire angle-of-attack range tested.

2. Small amounts of throat bleed to 4 percent caused slight decreases in inlet stability while further bleed increases to 8 percent resulted in large stability gains. For this larger bleed, the inlet mass-flow ratio was reduced almost to zero without experiencing instability. Large ranges of subcritical stability were maintained to an angle of attack of 20°.

3. Use of only 2-percent throat bleed yielded significant reductions in critical distortion (e.g., from 20 percent to slightly less than 10 percent at Mach number 2.0 and zero angle of attack). Further bleed provided only slight additional distortion improvements. Relatively low distortions were maintained to an angle of attack of 20°.

4. Ramp perforations provided slight increases in inlet pressure recovery and stability.

5. In general, the fuselage fences were not very effective with this top inlet which had throat bleed and which was closer to the nose than a previously investigated top inlet.

6. Above an angle of attack of 9.5° and at a free-stream Mach number of 2.0, the top inlets with the round approach performed considerably better than those having a flat approach.

7. At a free-stream Mach number of 2.0 both canopies (faired and unfaired) caused reductions in inlet pressure recovery at low angles of attack (0° and 5°). However, at angles greater than 9° the configurations with canopies gave pressure recoveries comparable to those without canopies but having the round approach.

8. The inlet side fairings increased both pressure recovery and mass flow several percent at the expense of a slight reduction in stability limits.

9. The simulated 60° delta wings caused slight decreases in both pressure recovery and stability at angle of attack.

Lewis Flight Propulsion Laboratory
National Advisory Committee for Aeronautics
Cleveland, Ohio, January 23, 1957

REFERENCES

1. Valerino, Alfred S., Pennington, Donald B., and Vargo, Donald J.: Effect of Circumferential Location on Angle of Attack Performance of Twin Half-Conical Scoop-Type Inlets Mounted Symmetrically on the RM-10 Body of Revolution. NACA RM E53G09, 1953.

2. Hasel, Lowell E., Lankford, John L., and Robins, A. W.: Investigation of a Half-Conical Scoop Inlet Mounted at Five Alternate Circumferential Locations Around a Circular Fuselage. Pressure-Recovery Results at a Mach Number of 2.01. NACA RM L53D03b, 1953.

3. Hasel, Lowell E.: The Performance of Conical Supersonic Scoop Inlets on Circular Fuselages. NACA RM L53I14a, 1953.

4. Kremzier, Emil J., and Campbell, Robert C.: Angle-of-Attack Supersonic Performance of a Configuration Consisting of a Ramp-Type Scoop Inlet Located Either on Top or Bottom of a Body of Revolution. NACA RM E54C09, 1954.

5. Kremzier, Emil J., and Campbell, Robert C.: Effect of Fuselage Fences on the Angle-of-Attack Supersonic Performance of a Top-Inlet - Fuselage Configuration. NACA RM E54J04, 1955.

6. Obery, Leonard J., and Cubbison, Robert W.: Effectiveness of Boundary-Layer Removal Near Throat of Ramp-Type Side Inlet at Free-Stream Mach Number of 2.0. NACA RM E54I14, 1954.

7. Obery, L. J., Cubbison, R. W., and Mercer, T. G.: Stabilization Techniques for Ramp-Type Side Inlets at Supersonic Speeds. NACA RM E55A26, 1955.

8. Stitt, Leonard E., Cubbison, Robert W., and Flaherty, Richard J.: Performance of Several Half-Conical Side Inlets at Supersonic and Subsonic Speeds. NACA RM E55J10a, 1956.

9. Stitt, Leonard E., McKevitt, Frank X., and Smith, Albert B.: Effect of Throat Bleed on Supersonic Performance of a Half-Conical Side-Inlet System. NACA RM E55J07, 1956.

10. Campbell, Robert C.: Performance of Supersonic Ramp-Type Side Inlet with Combinations of Fuselage and Inlet Throat Boundary-Layer Removal. NACA RM E56A17, 1956.

11. Allen, John L.: Performance of a Blunt-Lip Side Inlet with Ramp Bleed, Bypass, and a Long Constant-Area Duct Ahead of the Engine: Mach Numbers 0.66 and 1.5 to 2.1. NACA RM E56J01, 1956.

12. Simon, Paul C., Brown, Dennis W., and Huff, Ronald G.: Performance of External-Compression Bump Inlet at Mach Numbers of 1.5 to 2.0. NACA RM E56L19, 1957.

13. Allen, John L., and Piercy, Thomas G.: Performance Characteristics of an Underslung Vertical-Wedge with Porous Suction at Mach Numbers of 0.63 and 1.5 to 2.0. NACA RM E56B15, 1956.

14. Piercy, Thomas G., and Chiccine, Bruce G.: Development of Flow Distortions in a Full-Scale Nacelle Inlet at Mach Numbers 0.63 and 1.6 to 2.0. NACA RM E56G13a, 1956.

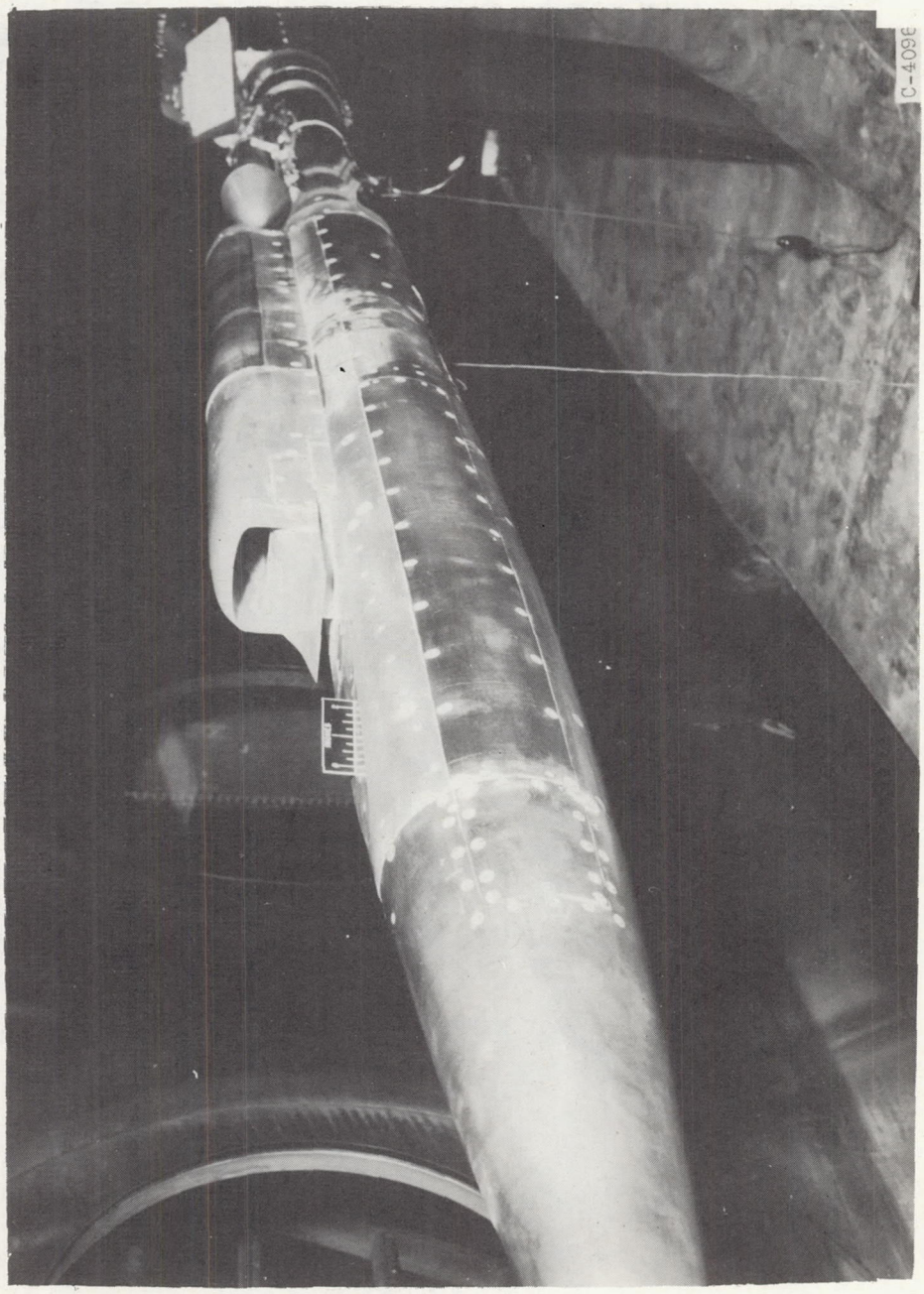

(a) Model in tunnel.

Figure 1. - Test configuration.

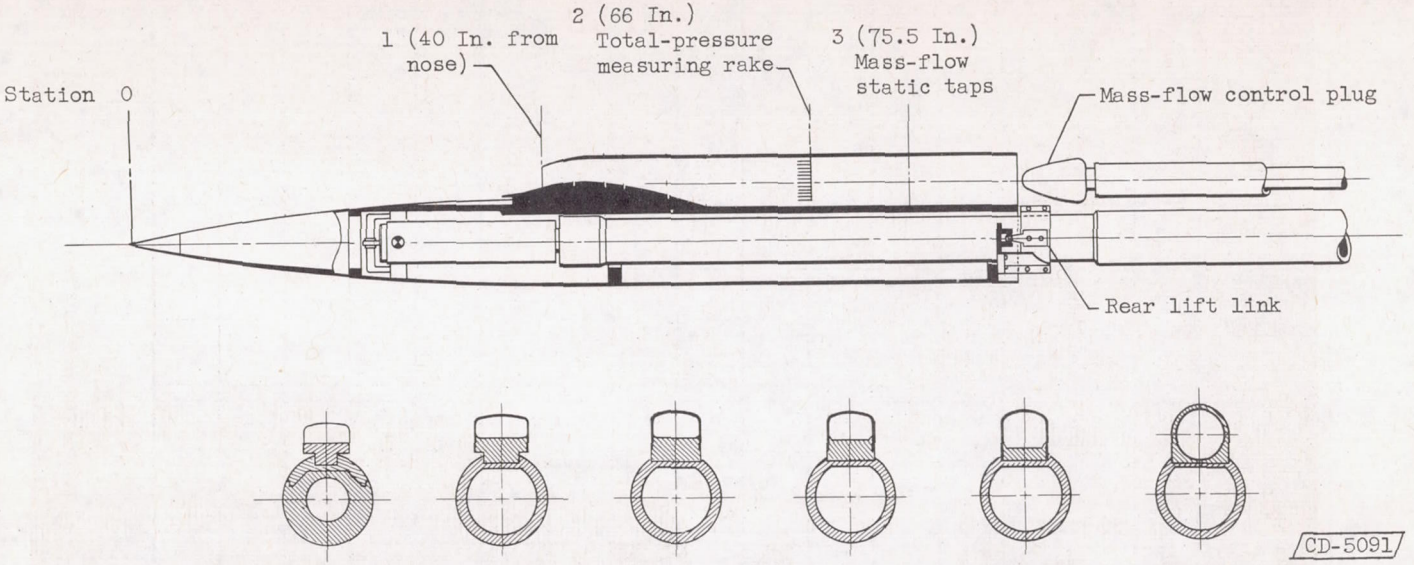

(b) Schematic drawing.

Figure 1. - Concluded. Test configuration.

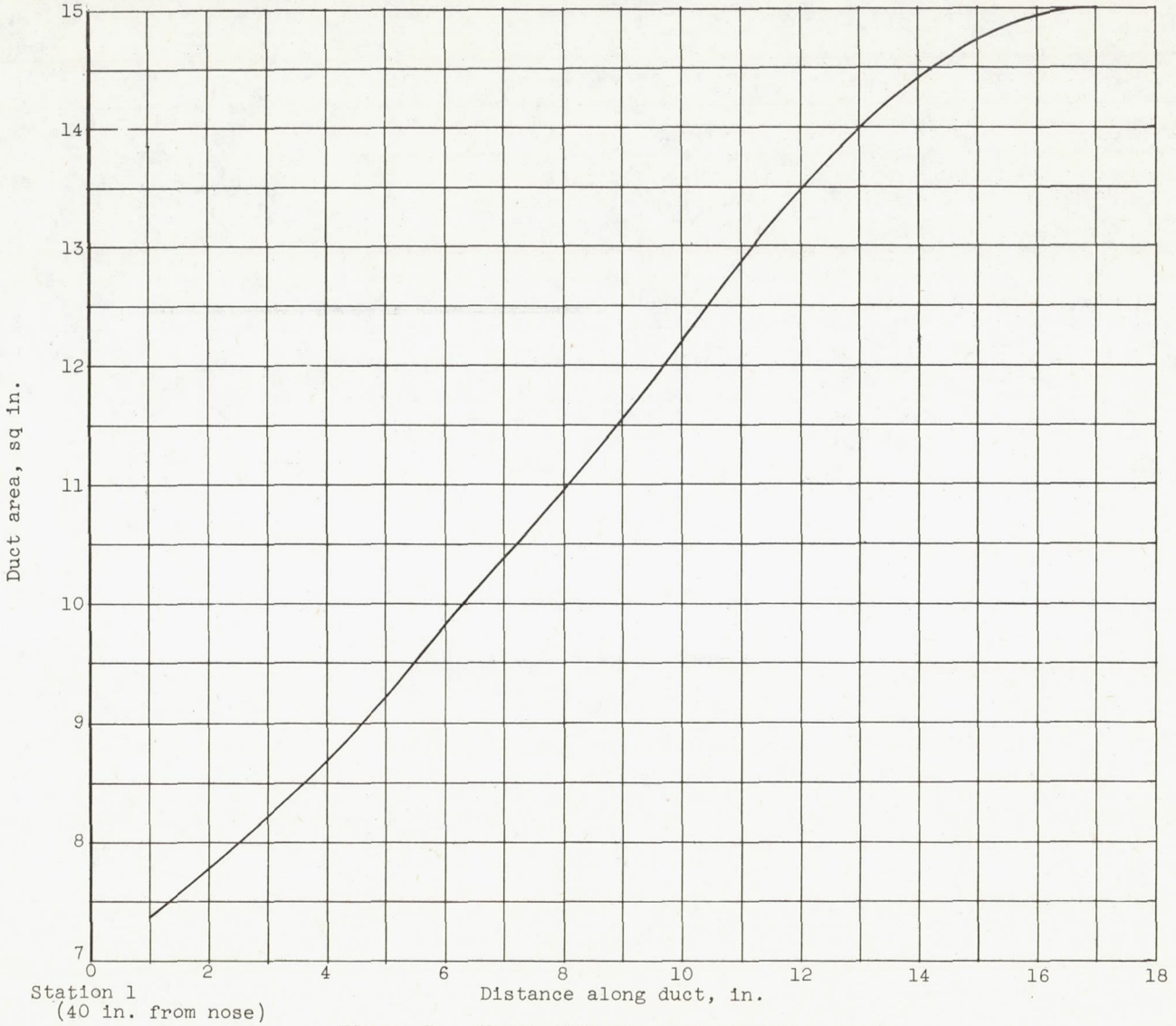

Figure 2. - Model diffuser-area variation curve.

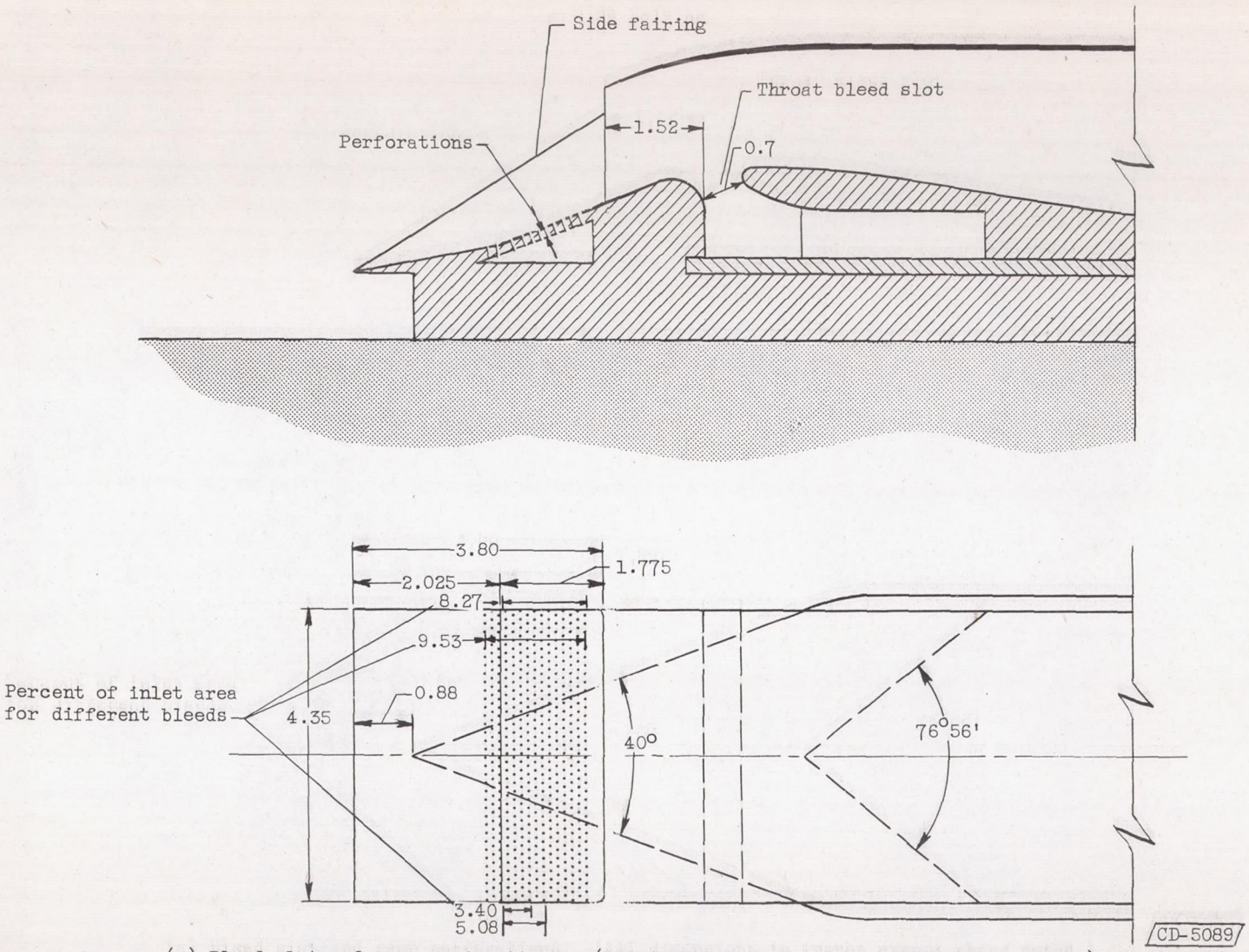

(a) Bleed slot and ramp perforations. (All dimensions in inches except where noted.)

Figure 3. - Inlet details.

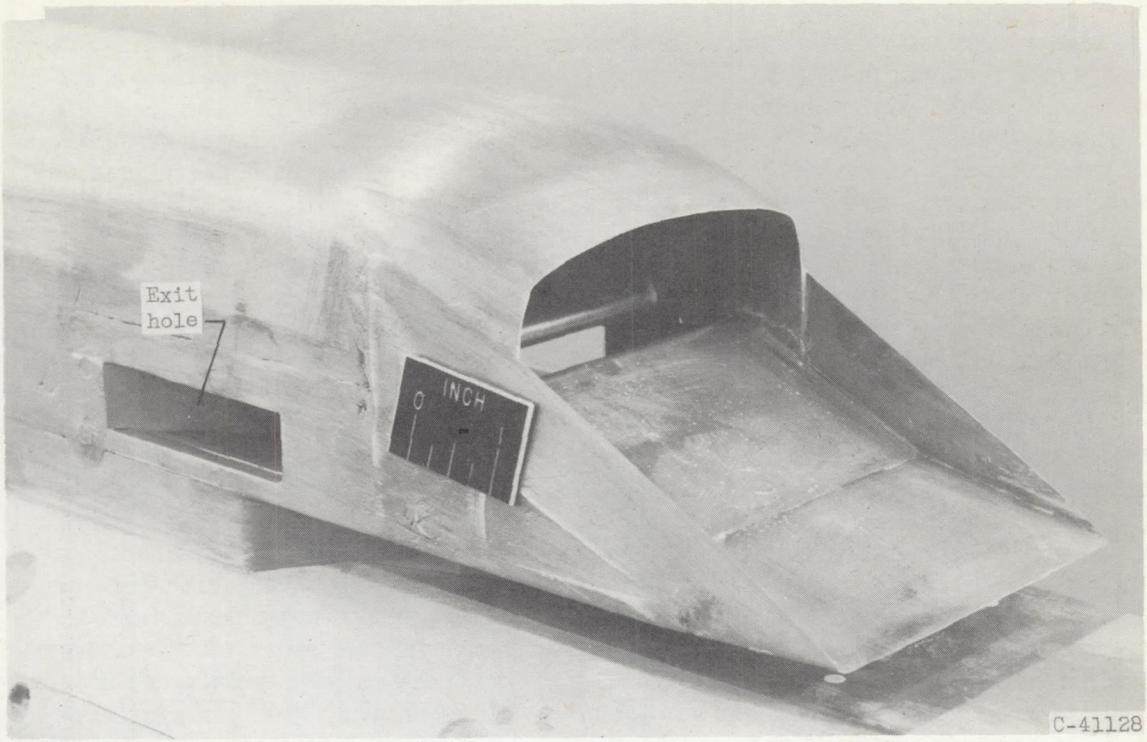

(b) Side fairings and flush slot bleed system; maximum bleed position.

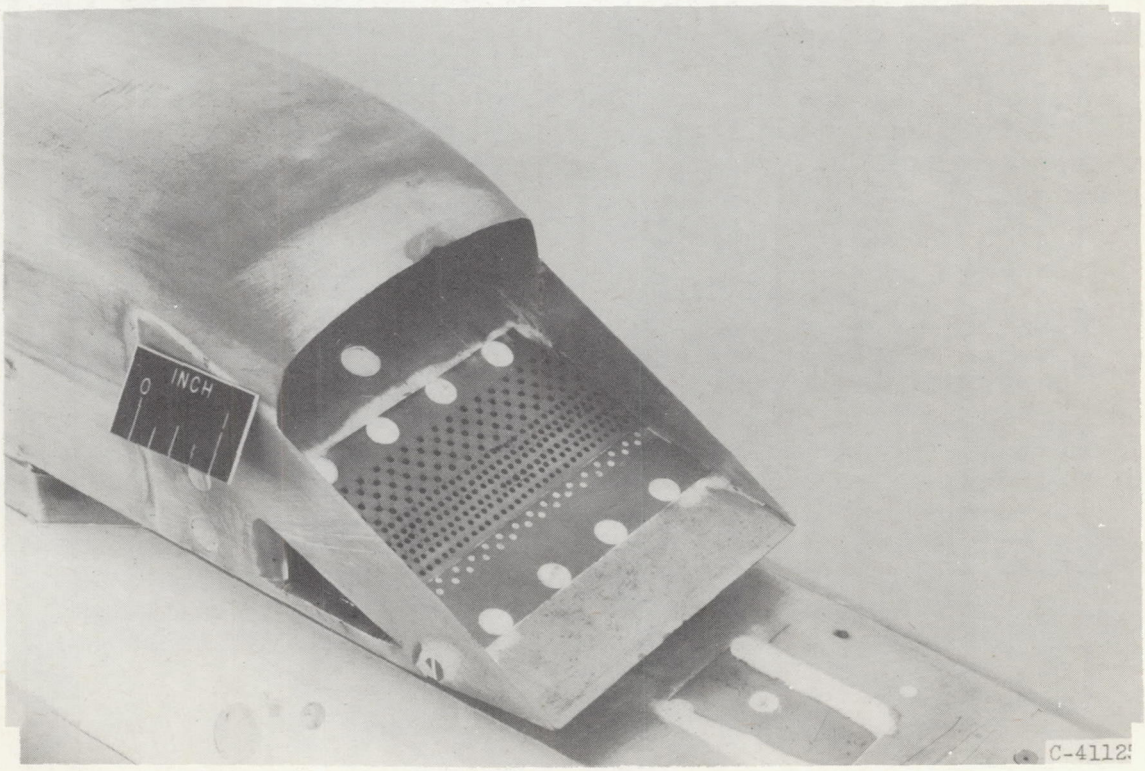

(c) Ramp perforations.

Figure 3. - Continued. Inlet details.

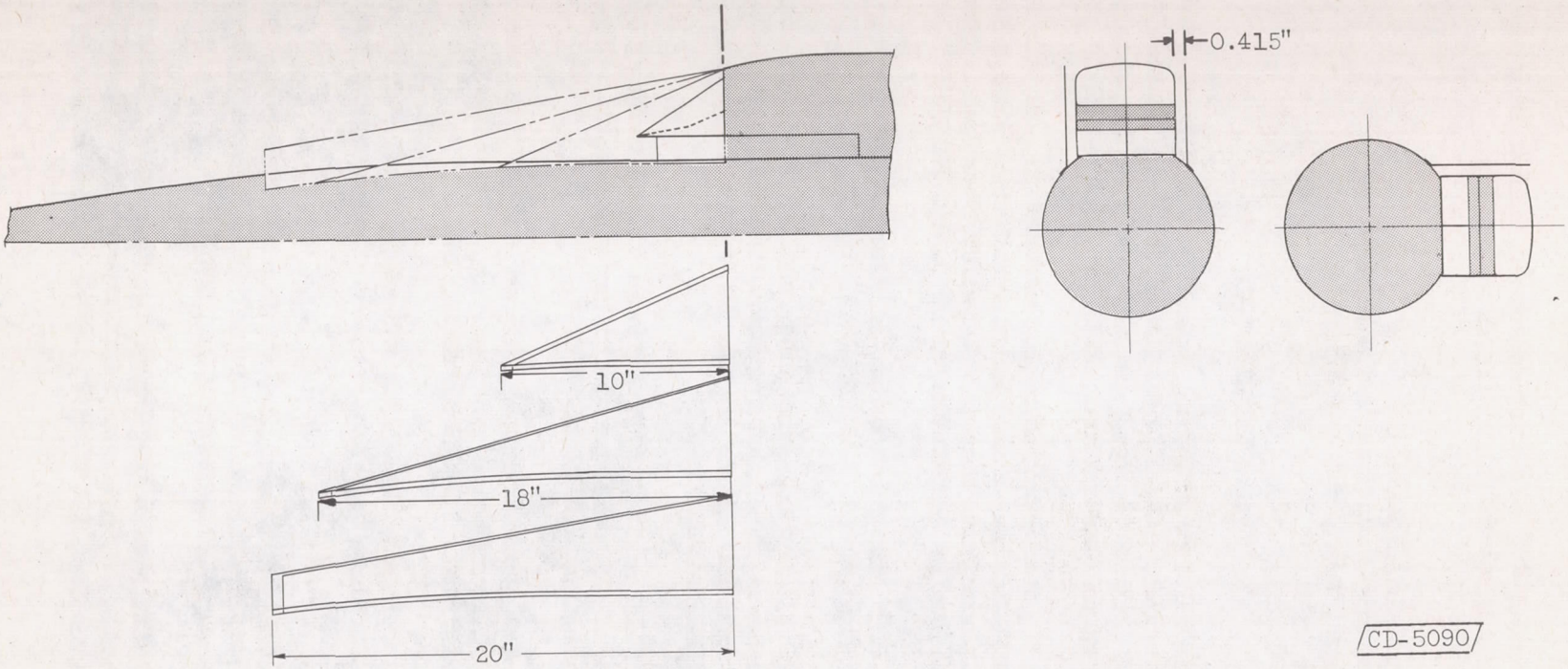

(d) Size and location of inlet fences.

Figure 3. - Continued. Inlet details.

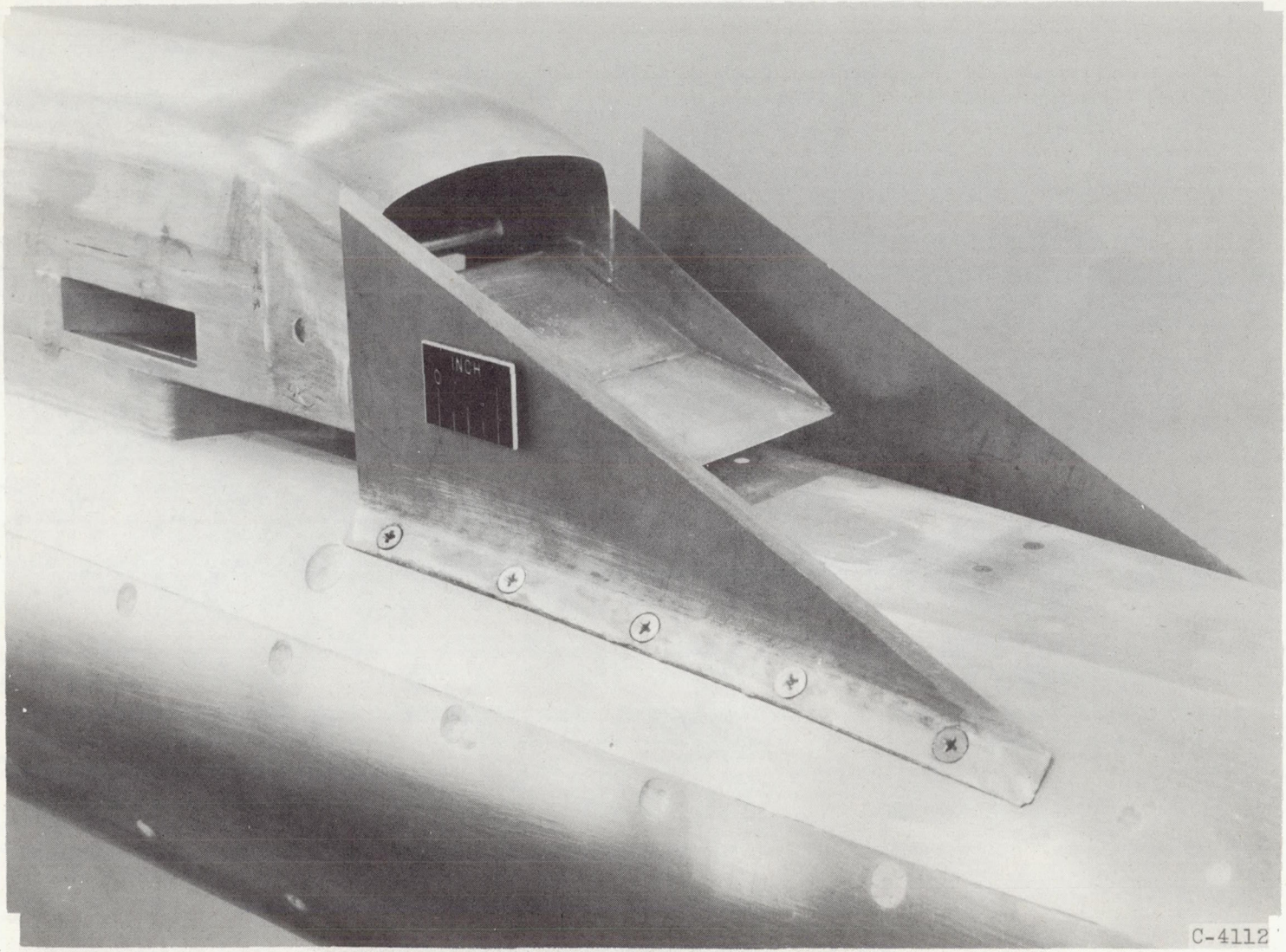

(e) Inlet with short fences.

Figure 3. - Concluded. Inlet details.

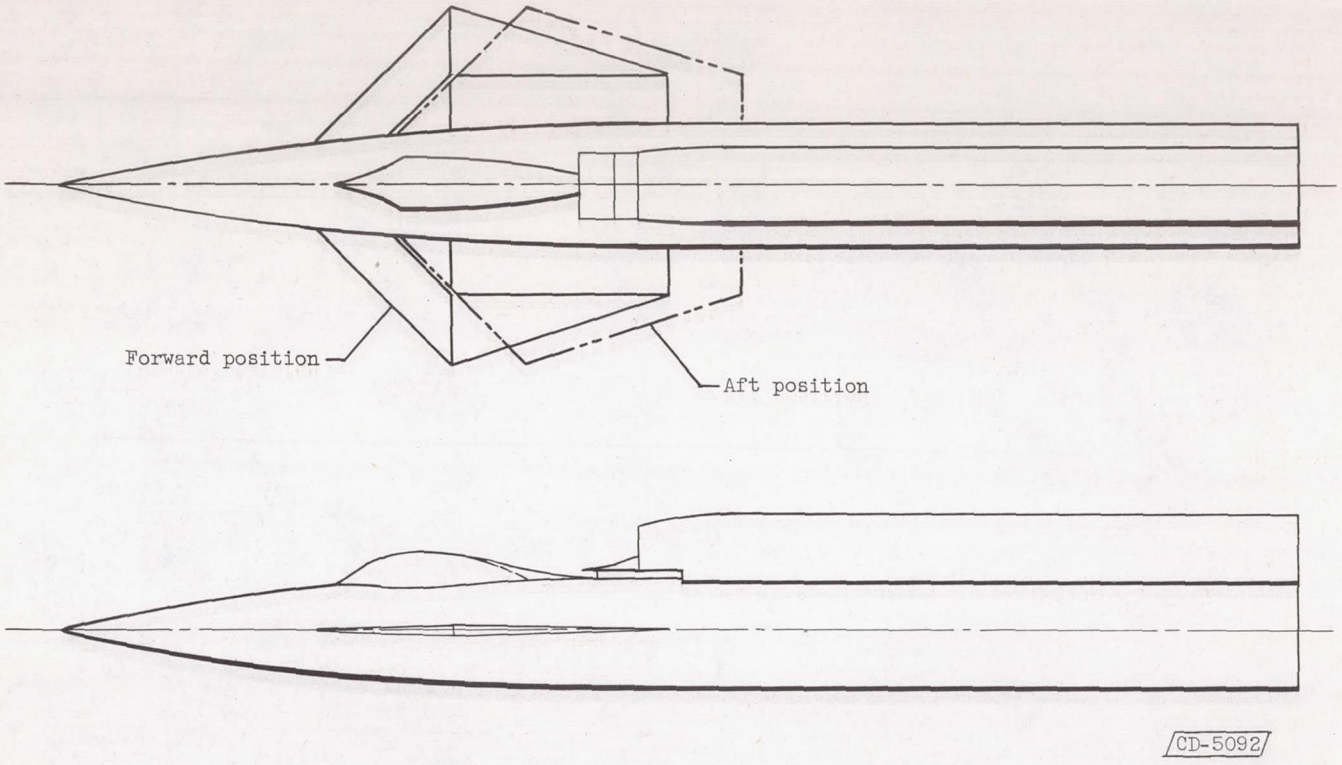

(a) Schematic drawing in positions tested.

Figure 4. - Canopy and wings.

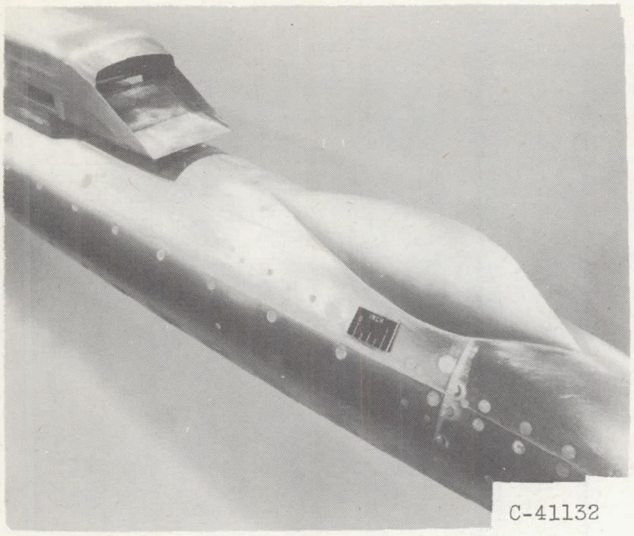

(b) Unfaired canopy.

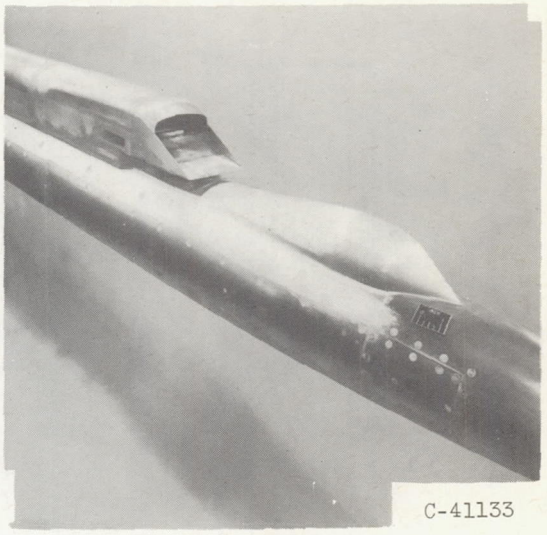

(c) Faired canopy.

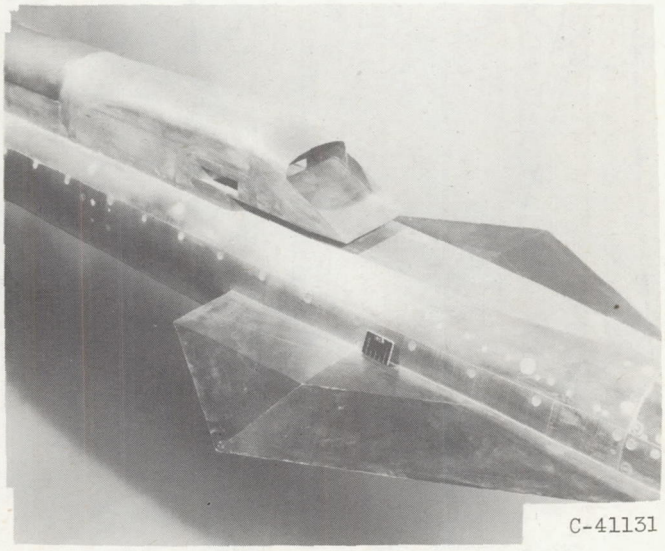

(d) Wing in forward position.

Figure 4. - Concluded. Canopy and wings.

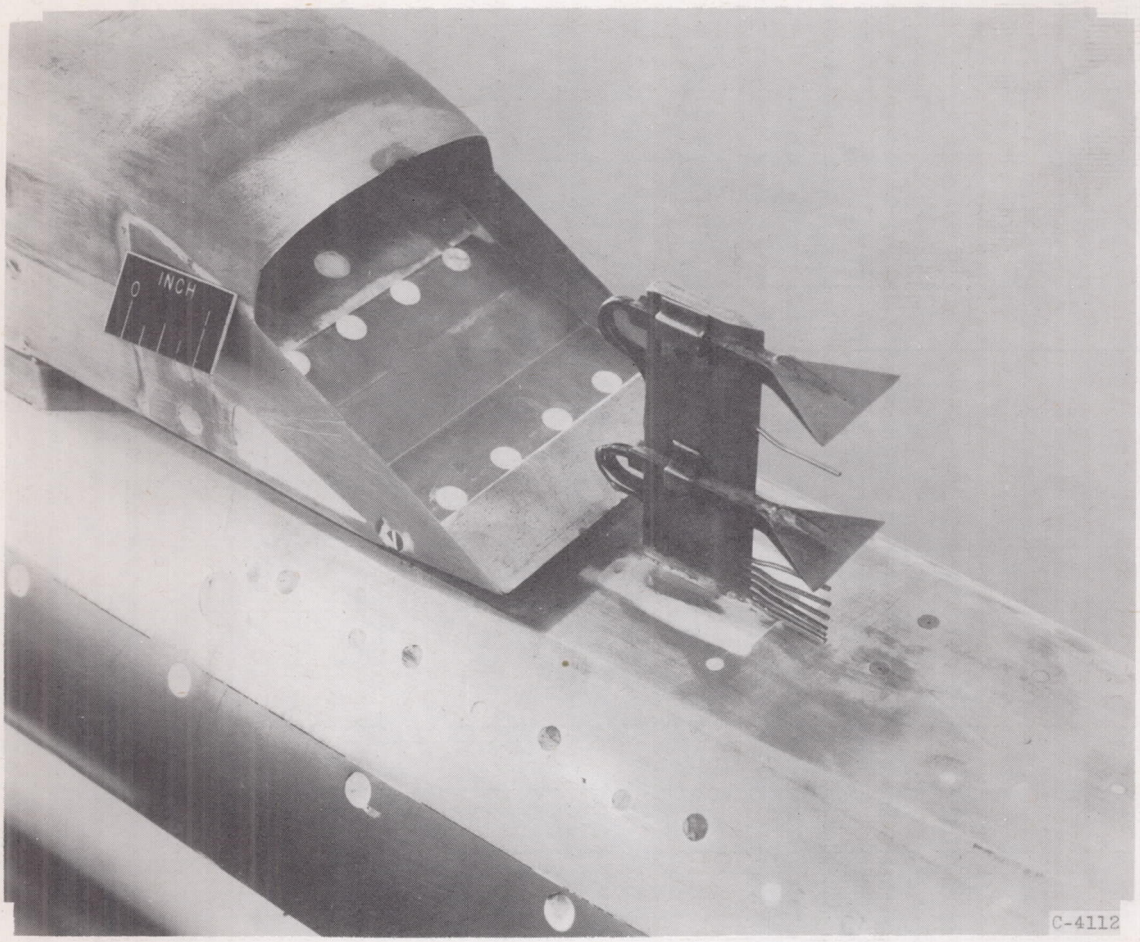

(a) Survey rake and wedges.

Figure 5. - Fuselage flow survey.

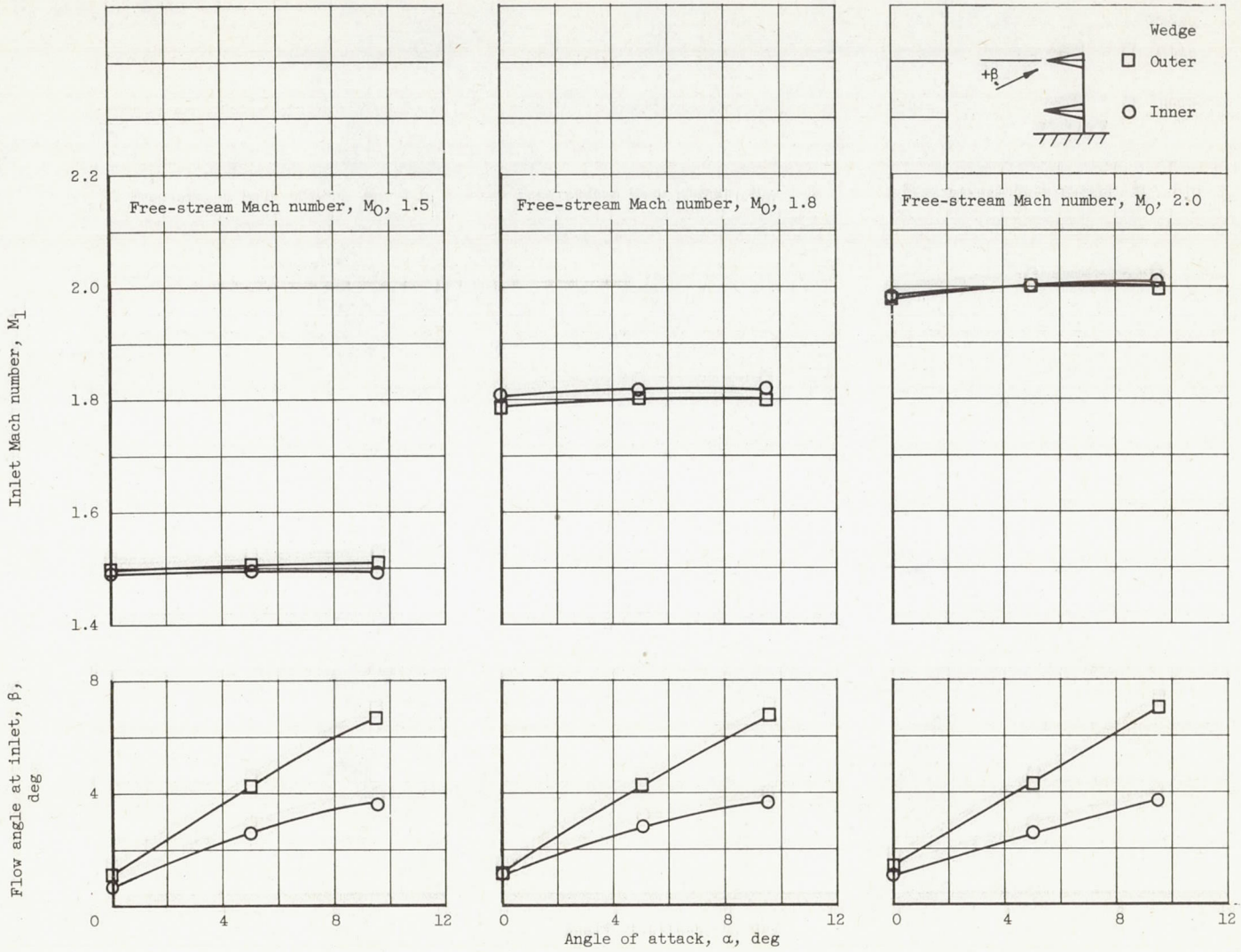

(b) Flat inlet approach.

Figure 5. - Continued. Fuselage flow survey.

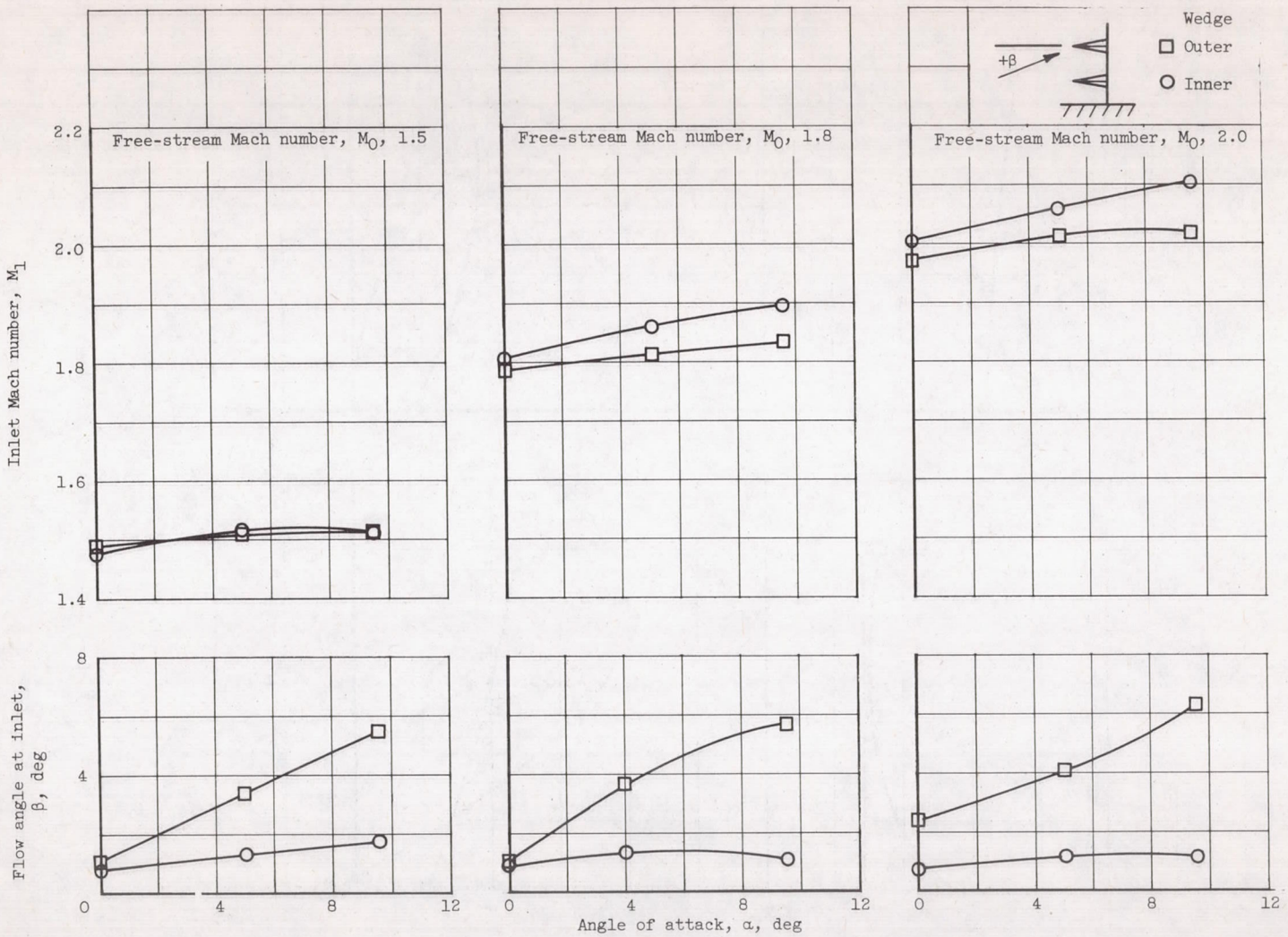

(c) With medium fence.

Figure 5. - Continued. Fuselage flow survey.

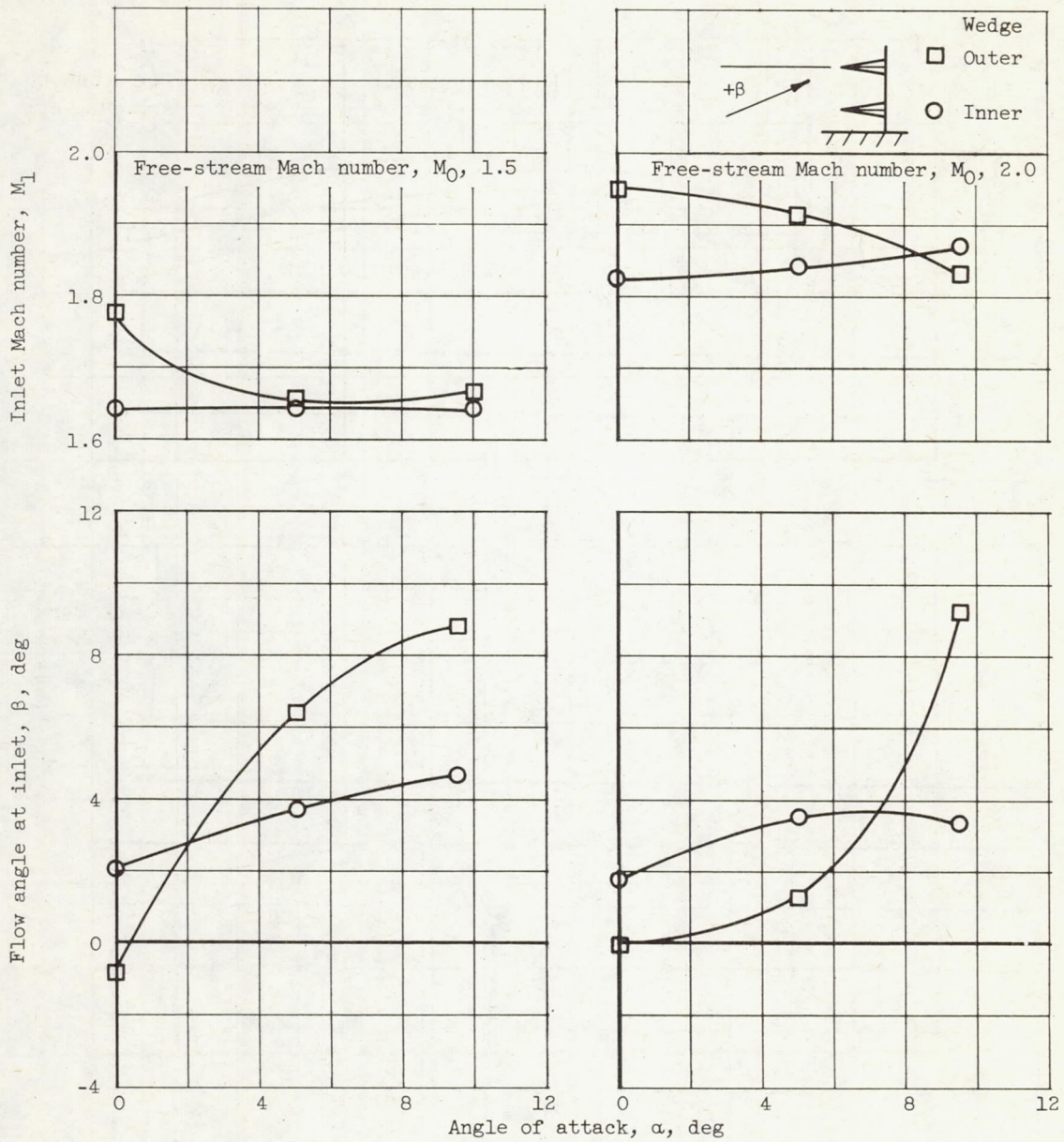

(d) With canopy.

Figure 5. - Continued. Fuselage flow survey.

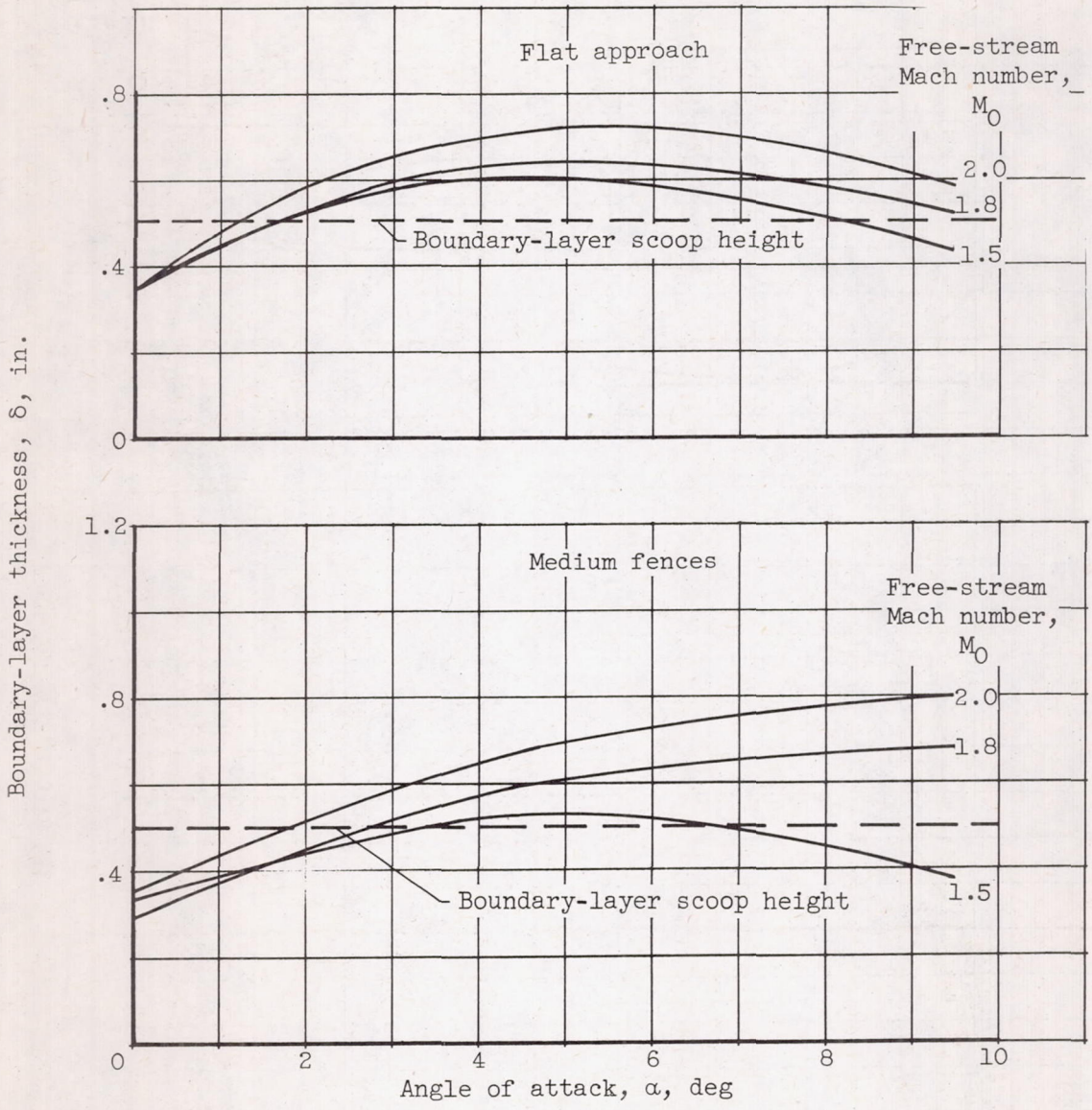

(e) Boundary-layer thickness.

Figure 5. - Concluded. Fuselage flow survey.

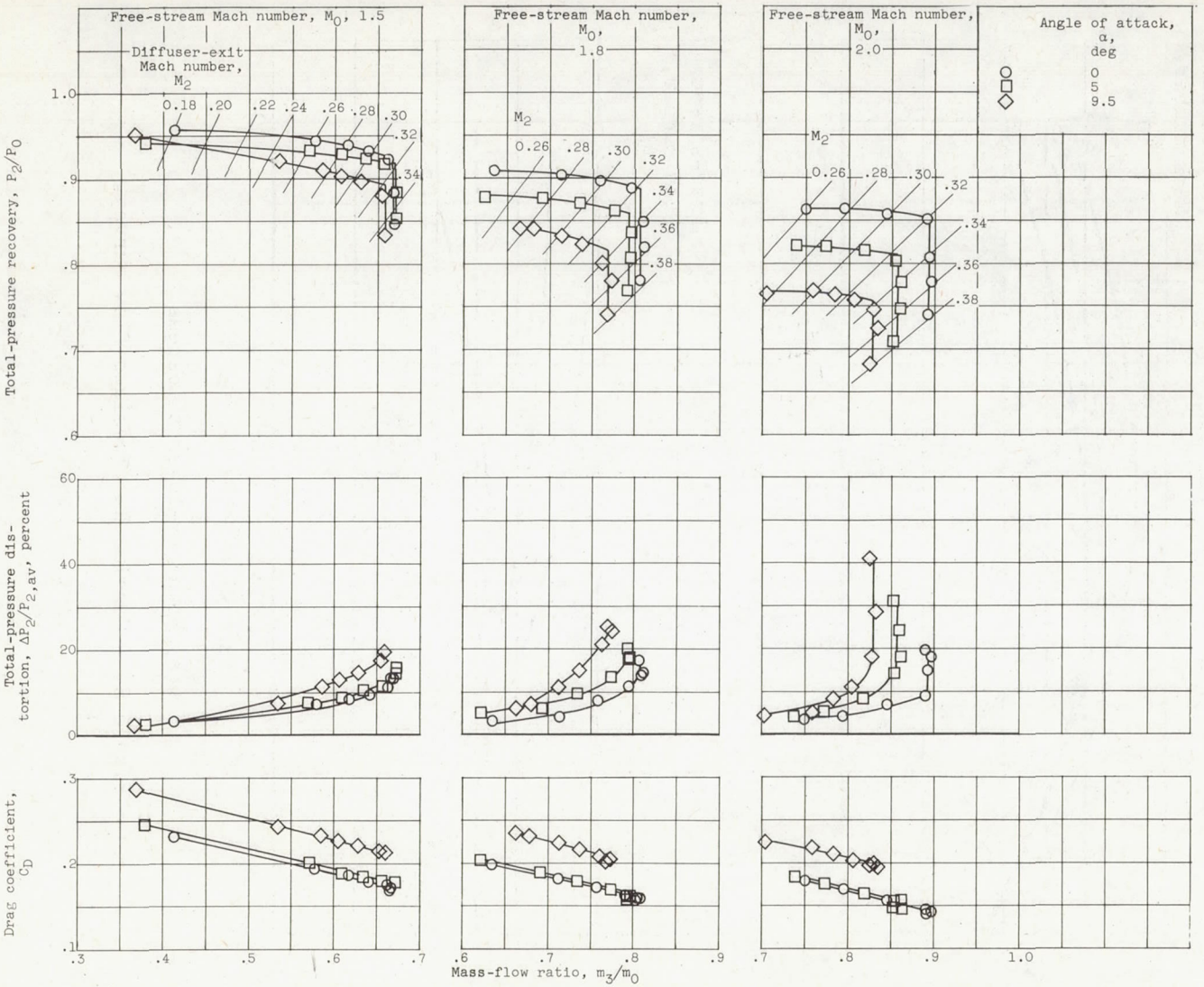

(a) Without side fairings.

Figure 6. - Inlet performance without bleed.

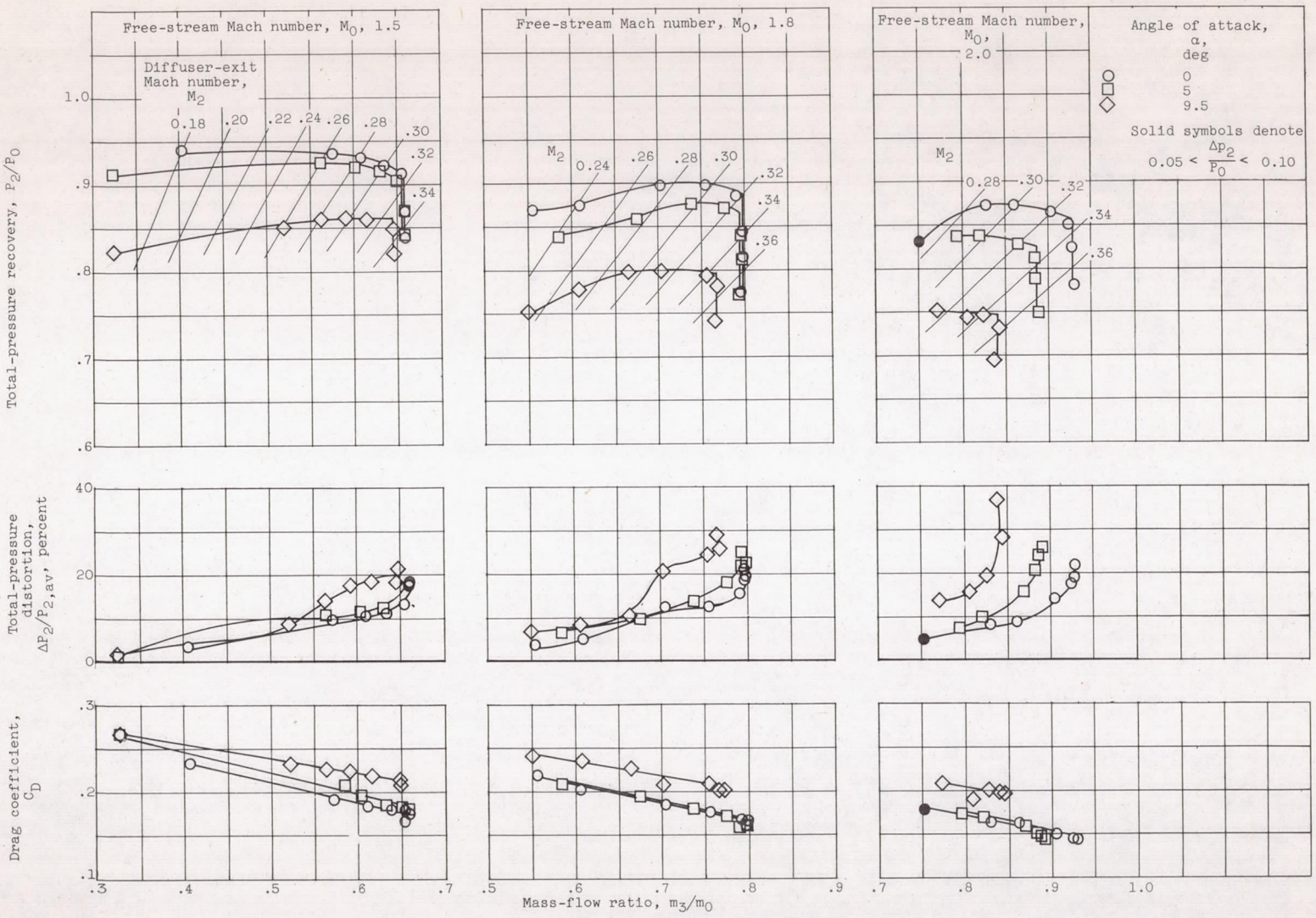

(b) With side fairings.

Figure 6. - Concluded. Inlet performance without bleed.

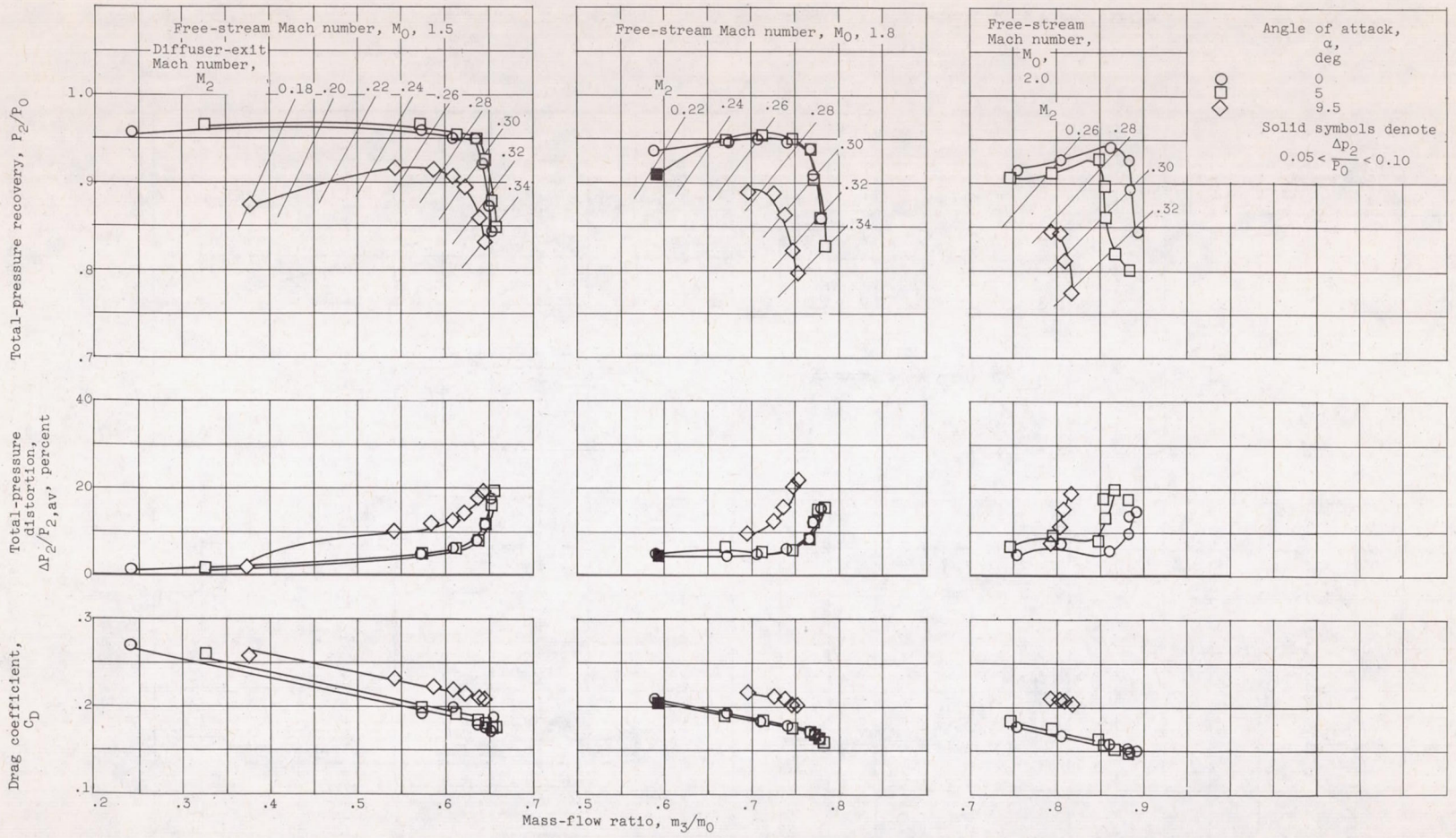

(a) 2-Percent bleed.

Figure 7. - Inlet performance with bleed and with side fairings.

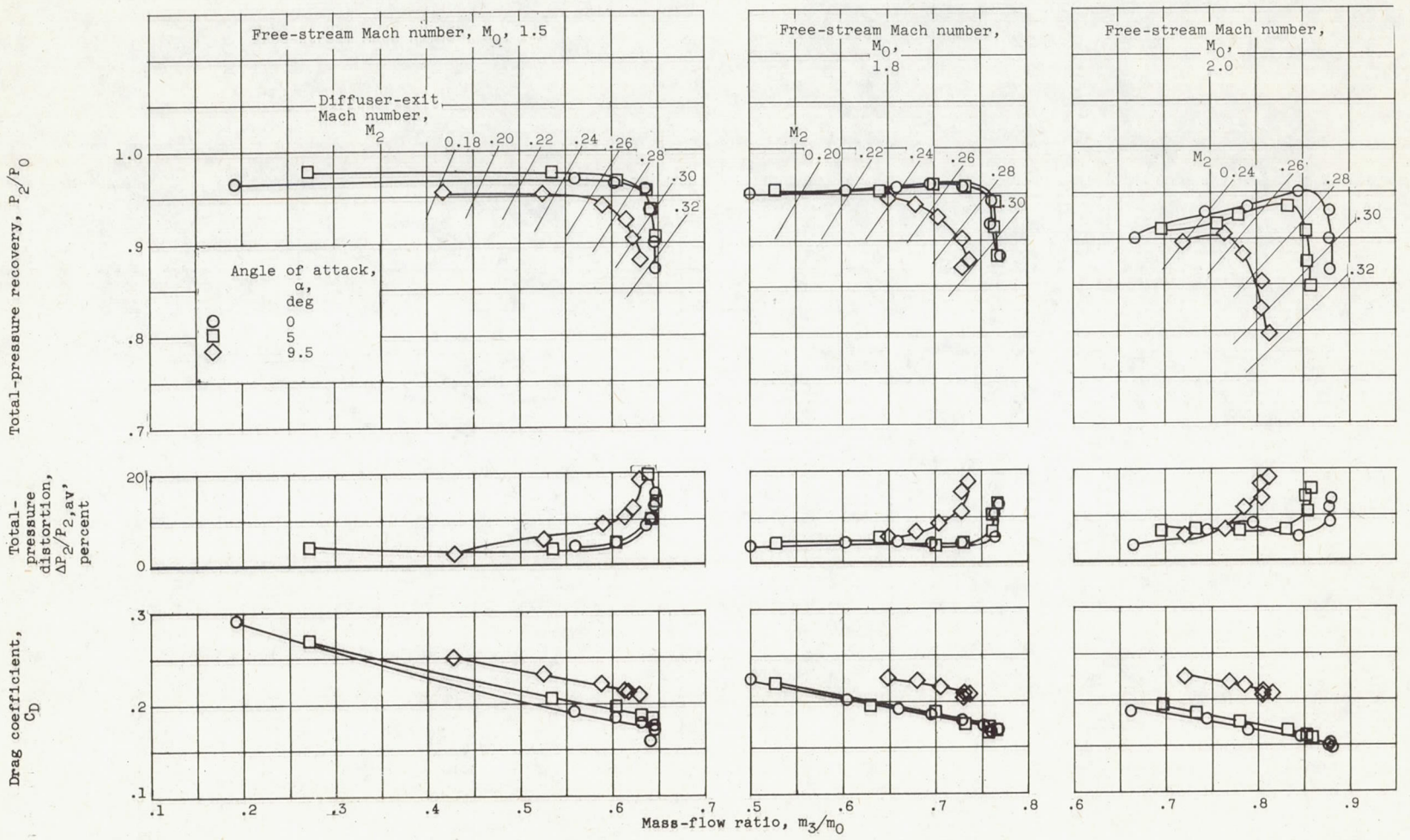

(b) 4-Percent bleed.

Figure 7. - Continued. Inlet performance with bleed and with side fairings.

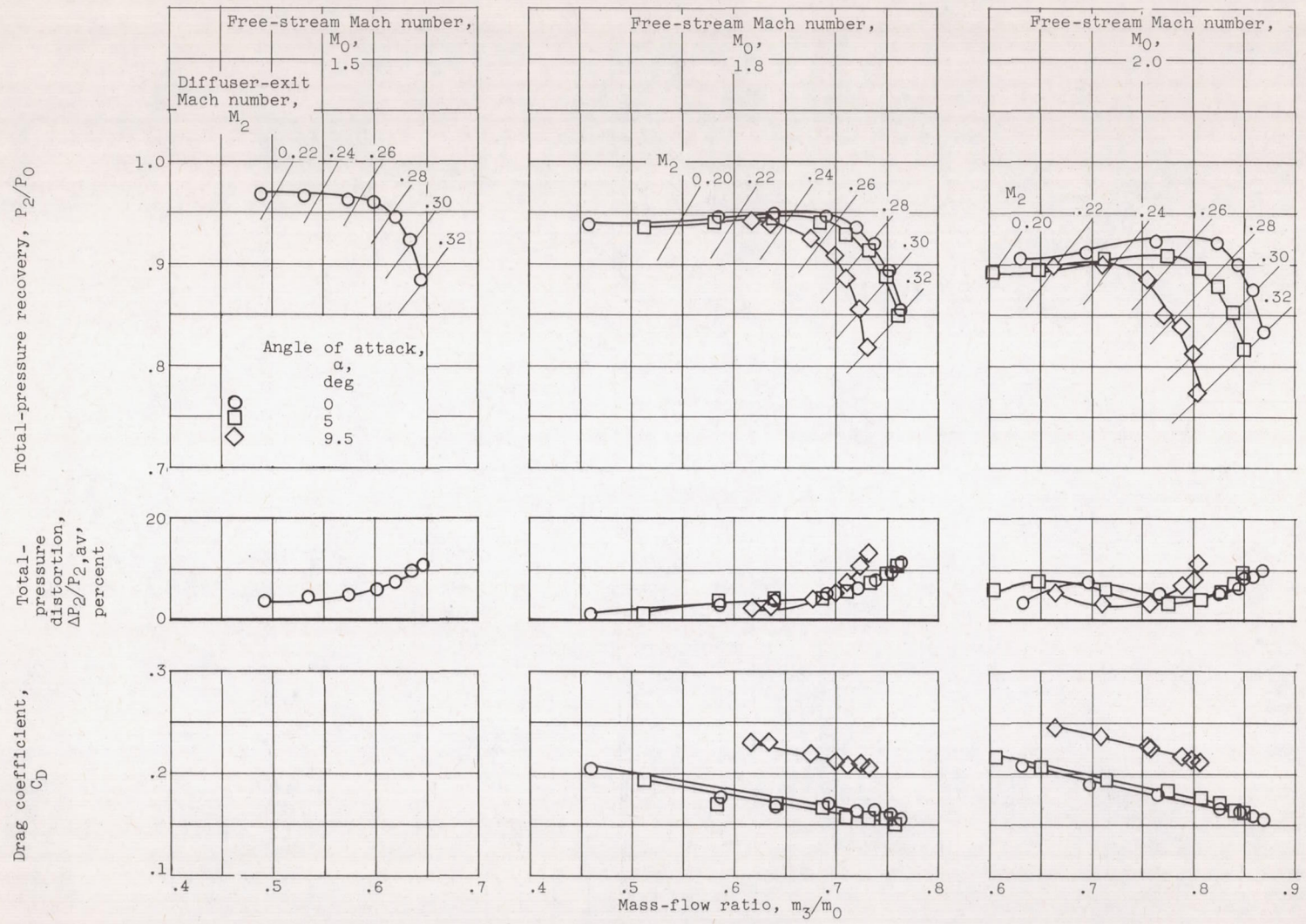

(c) 6-Percent bleed (obtained by partially closed throat slot).

Figure 7. - Continued. Inlet performance with bleed and with side fairings.

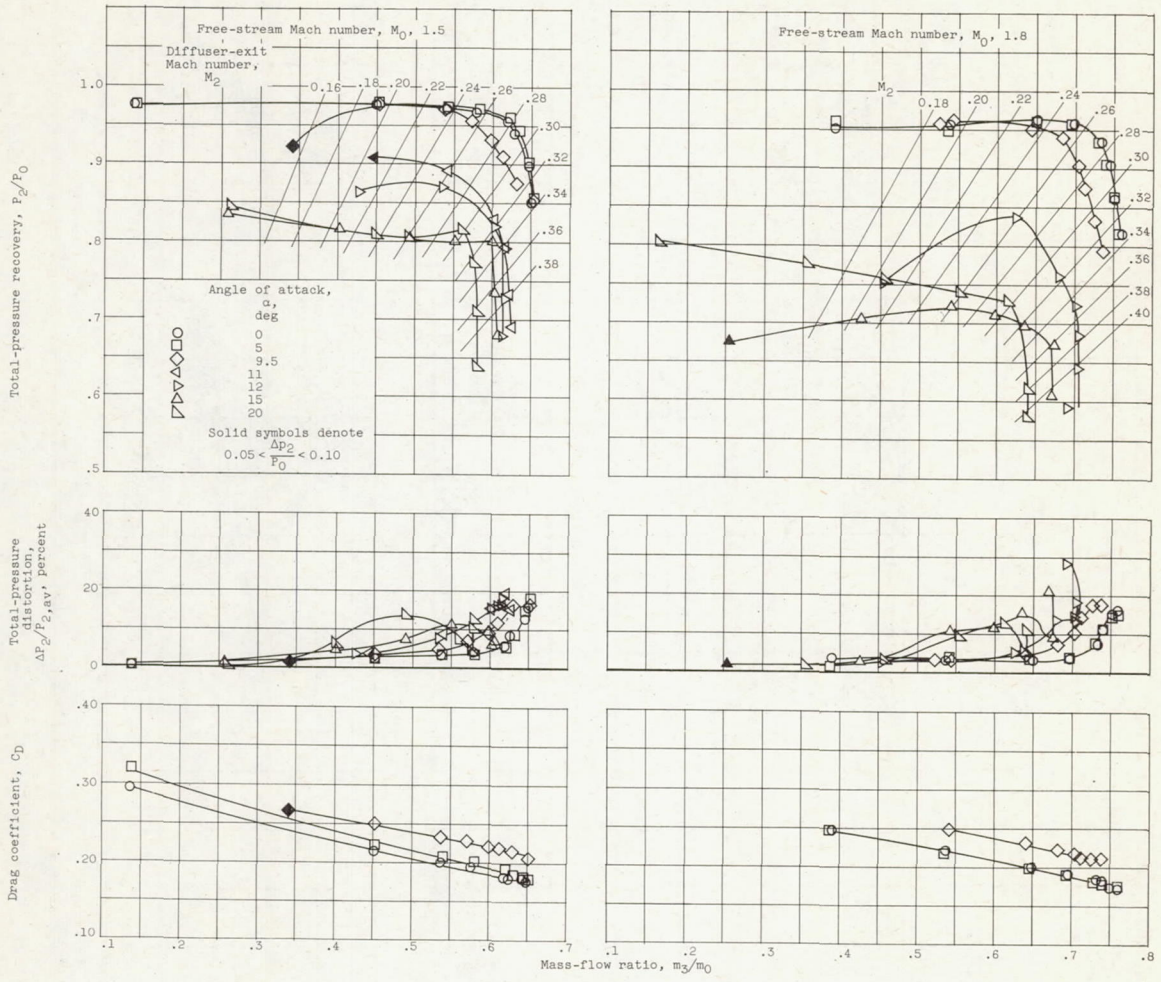

(d) 8-Percent bleed.

Figure 7. - Continued. Inlet performance with bleed and with side fairings.

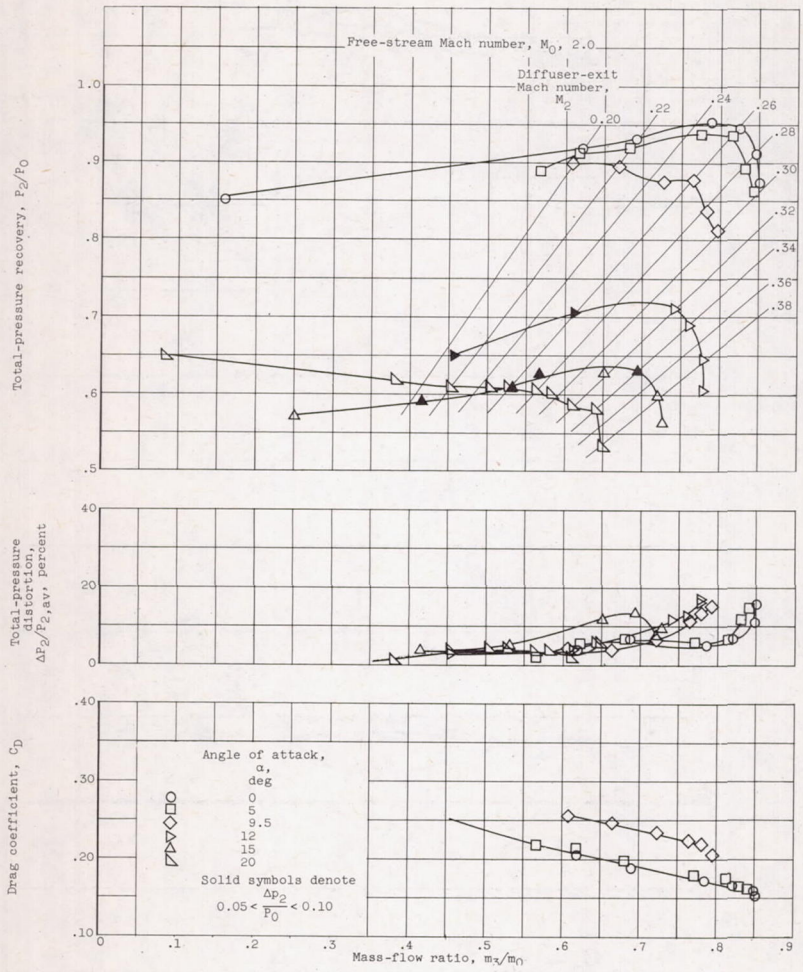

(d) Concluded. 8-percent bleed.

Figure 7. - Concluded. Inlet performance with bleed and with side fairings.

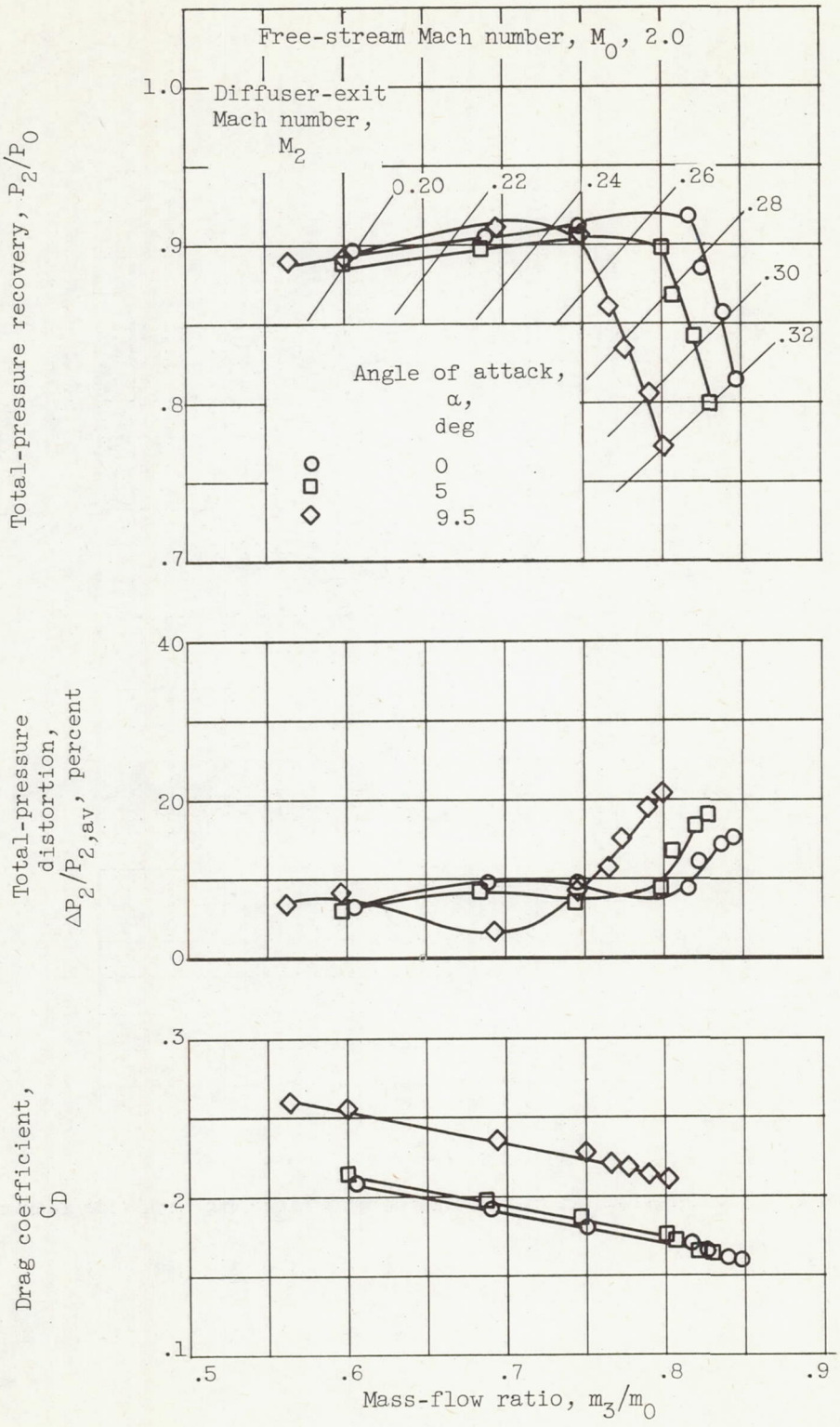

Figure 8. - Maximum bleed (8 percent) without side fairings.

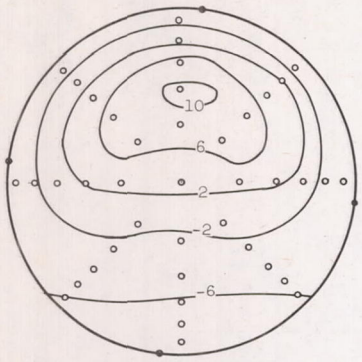

Mass-flow ratio, 0.925; total-pressure ratio, 0.850; total-pressure distortion, 17.74 percent; angle of attack, 0°

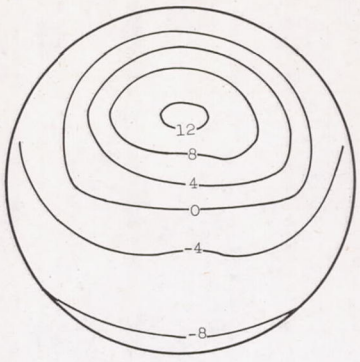

Mass-flow ratio, 0.884; total-pressure ratio, 0.812; total-pressure distortion, 20.06 percent; angle of attack, 5°

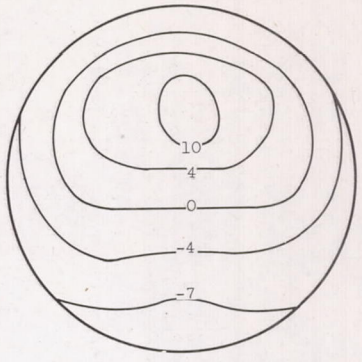

Mass-flow ratio, 0.825; total-pressure ratio, 0.745; total-pressure distortion, 19.0 percent; angle of attack, 9.5°

(a) Effect of angle of attack. Side fairings; no bleed; free-stream Mach number, 2.0.

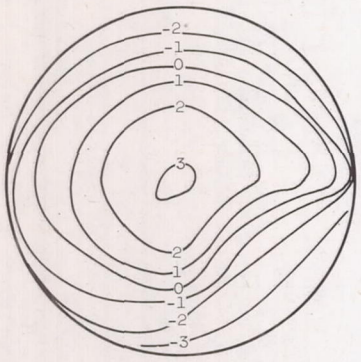

Mass-flow ratio, 0.822; total-pressure ratio, 0.944; total-pressure distortion, 6.70 percent; angle of attack, 0°

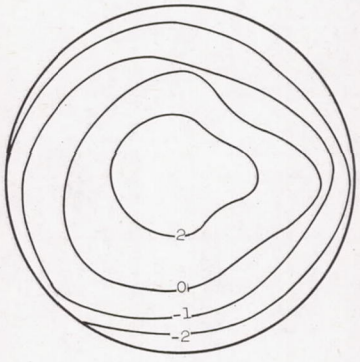

Mass-flow ratio, 0.815; total-pressure ratio, 0.935; total-pressure distortion, 6.31 percent; angle of attack, 5°

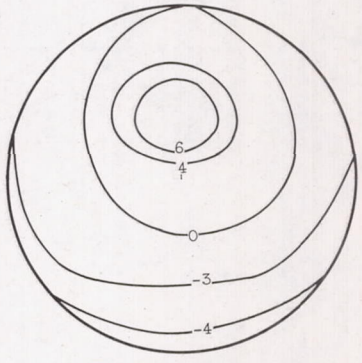

Mass-flow ratio, 0.764; total-pressure ratio, 0.877; total-pressure distortion, 11.30 percent; angle of attack, 9.5°

(b) Effect of angle of attack. Side fairings; 8-percent throat bleed; free-stream Mach number, 2.0.

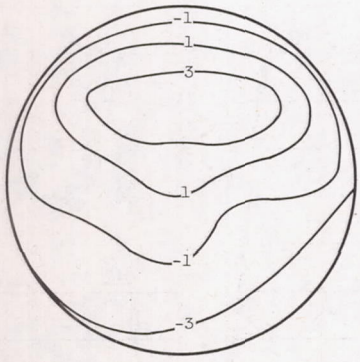

Mass-flow ratio, 0.733; total-pressure ratio, 0.936; total-pressure distortion, 7.38 percent; free-stream Mach number, 1.8

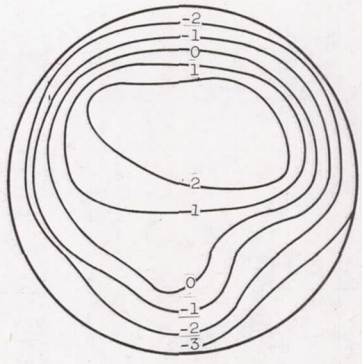

Mass-flow ratio, 0.643; total-pressure ratio, 0.956; total-pressure distortion, 5.97 percent; free-stream Mach number, 1.5

(c) Effect of free-stream Mach number. Side fairings; 8-percent throat bleed; angle of attack, 0°.

Figure 9. - Diffuser-exit total-pressure contours near critical flow for various top-inlet configurations.

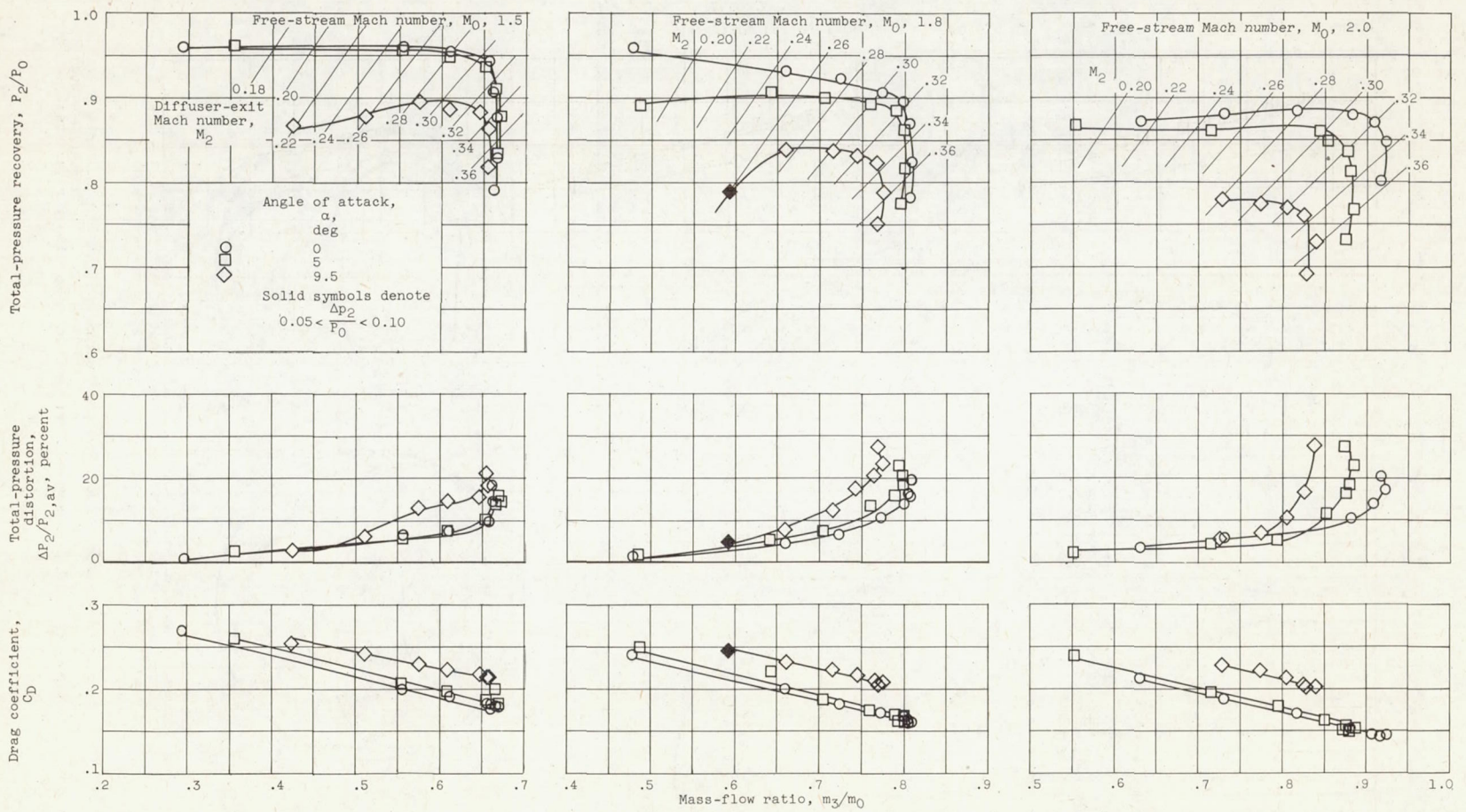

(a) 3.4 Percent of capture area.

Figure 10. - Inlet performance with ramp perforations plus side fairings.

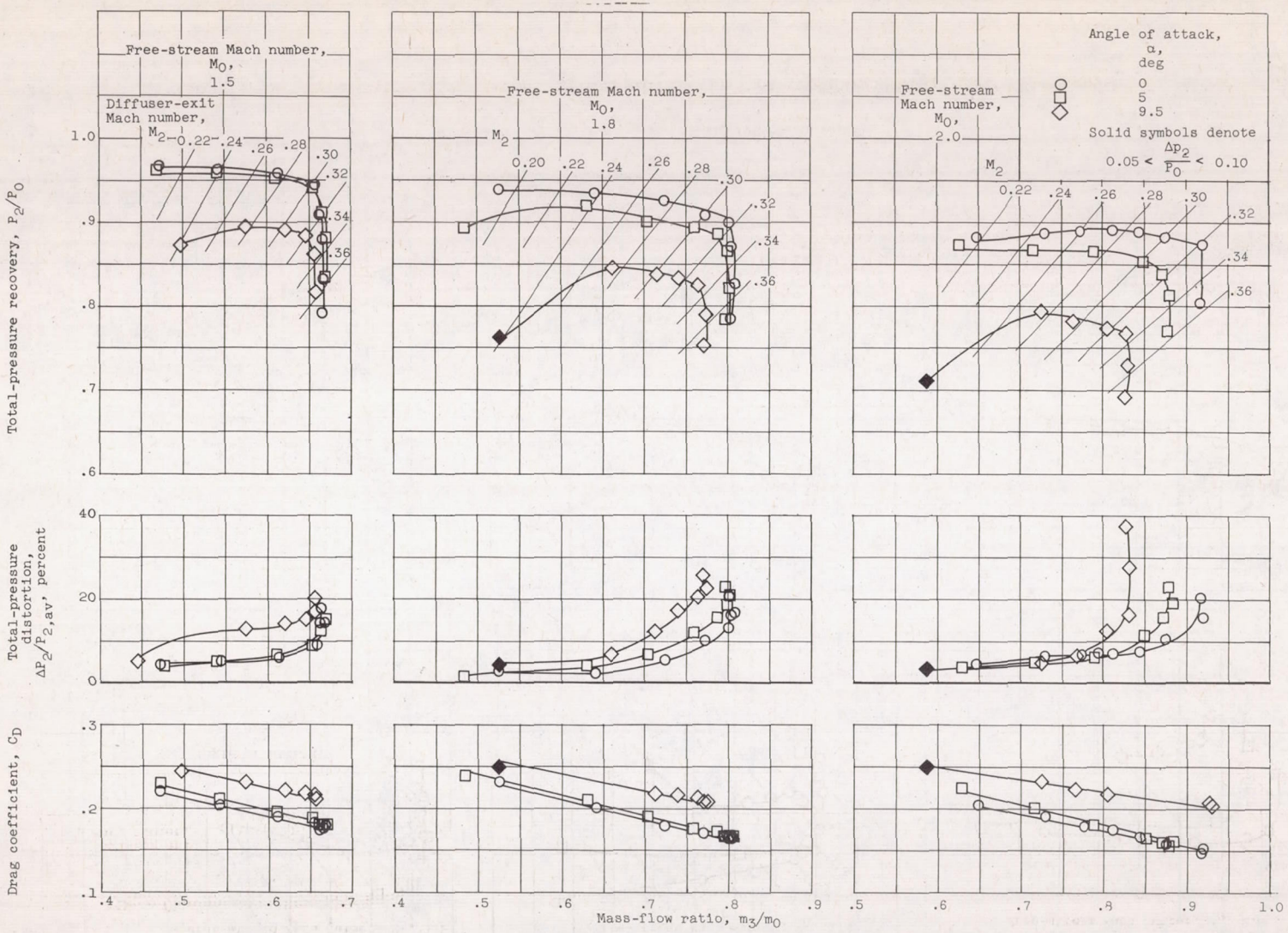

(b) 5.08 Percent of capture area.

Figure 10. - Continued. Inlet performance with ramp perforations plus side fairings.

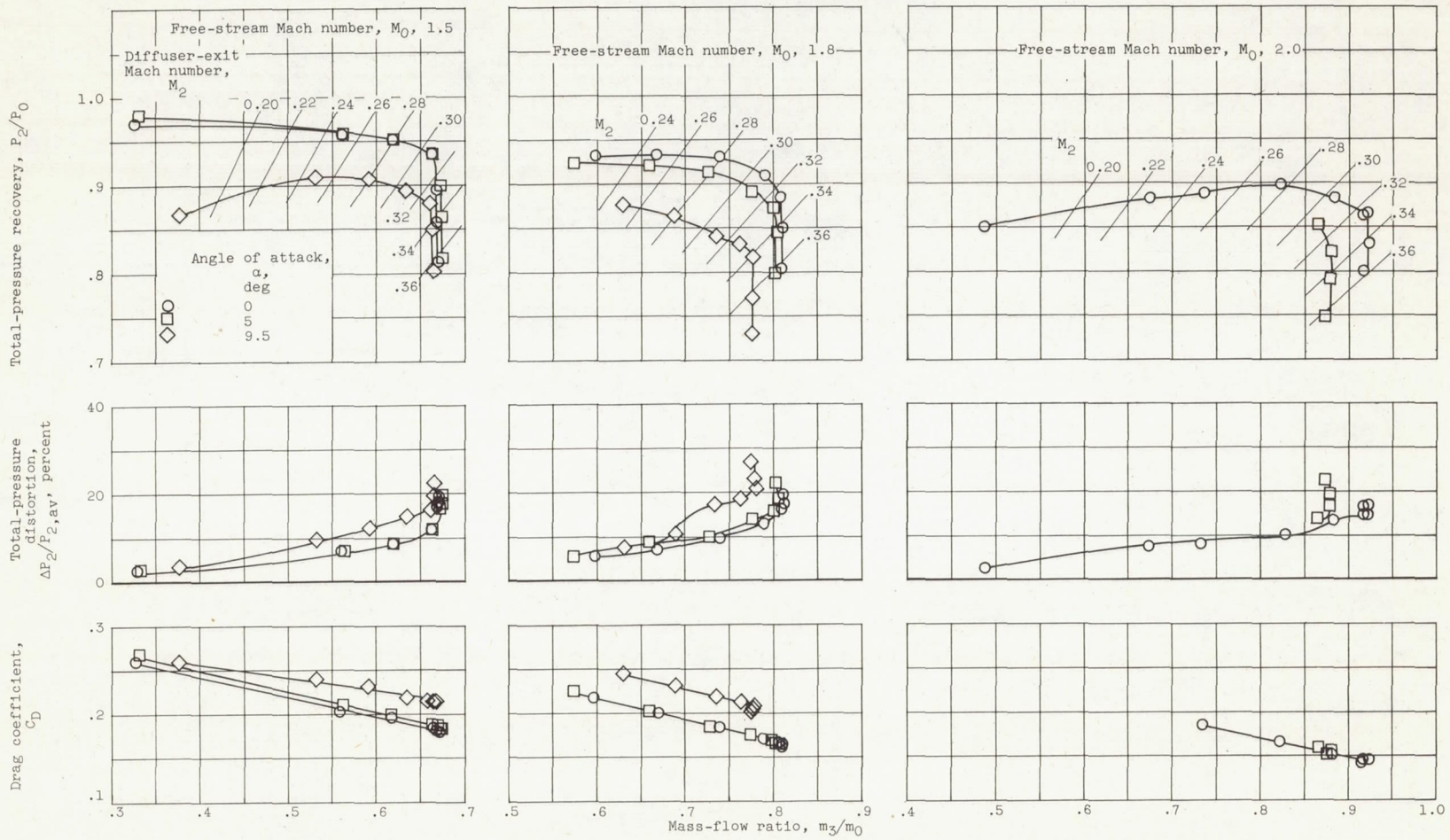

(c) 8.27 Percent of capture area.

Figure 10. - Continued. Inlet performance with ramp perforations plus side fairings.

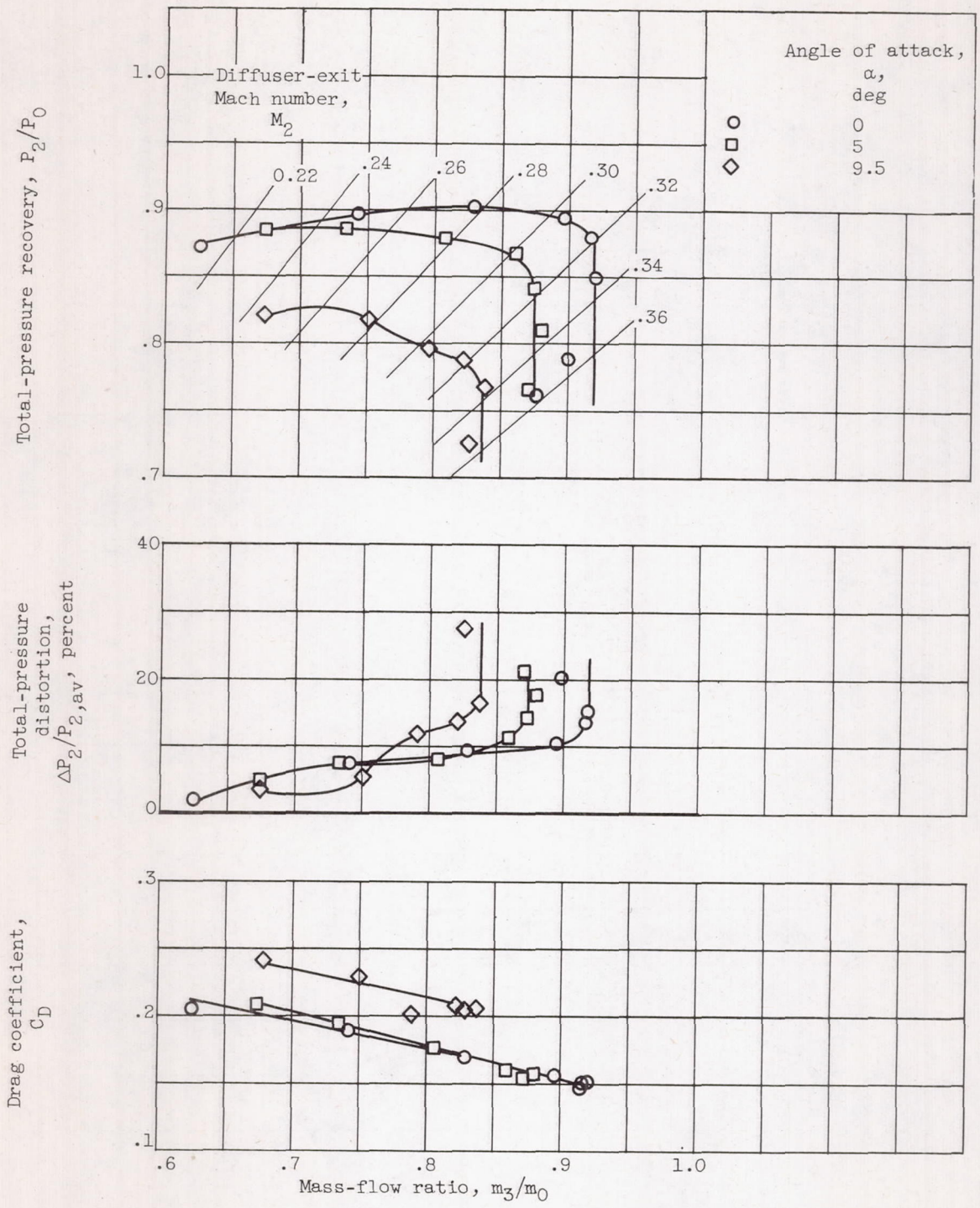

(d) 9.53 Percent of capture area. Free-stream Mach number, 2.0.

Figure 10. - Concluded. Inlet performance with ramp perforations plus side fairings.

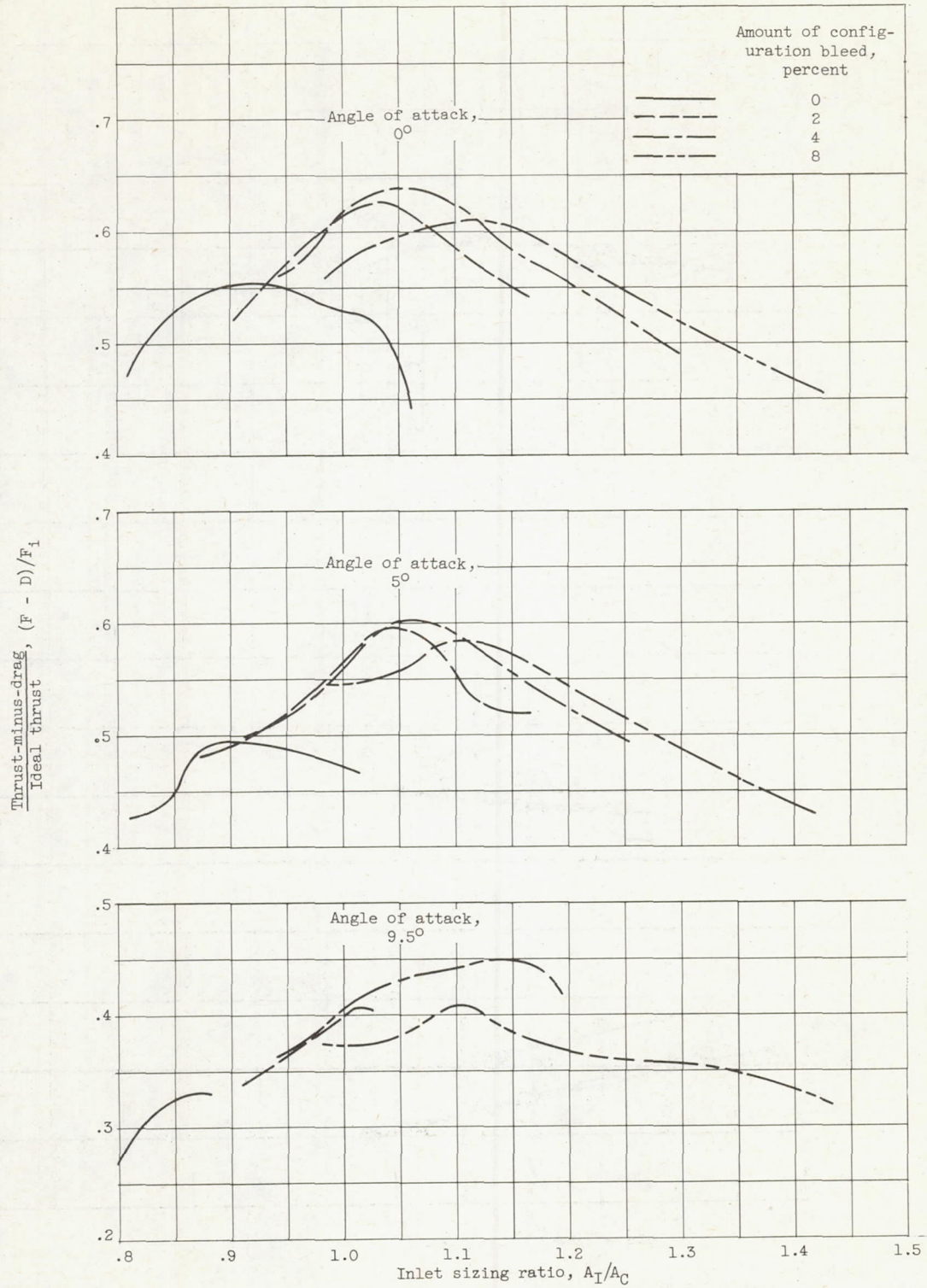

(a) Thrust-minus-drag comparison.

Figure 11. - Performance summary of bleed configurations at free-stream Mach number of 2.0.

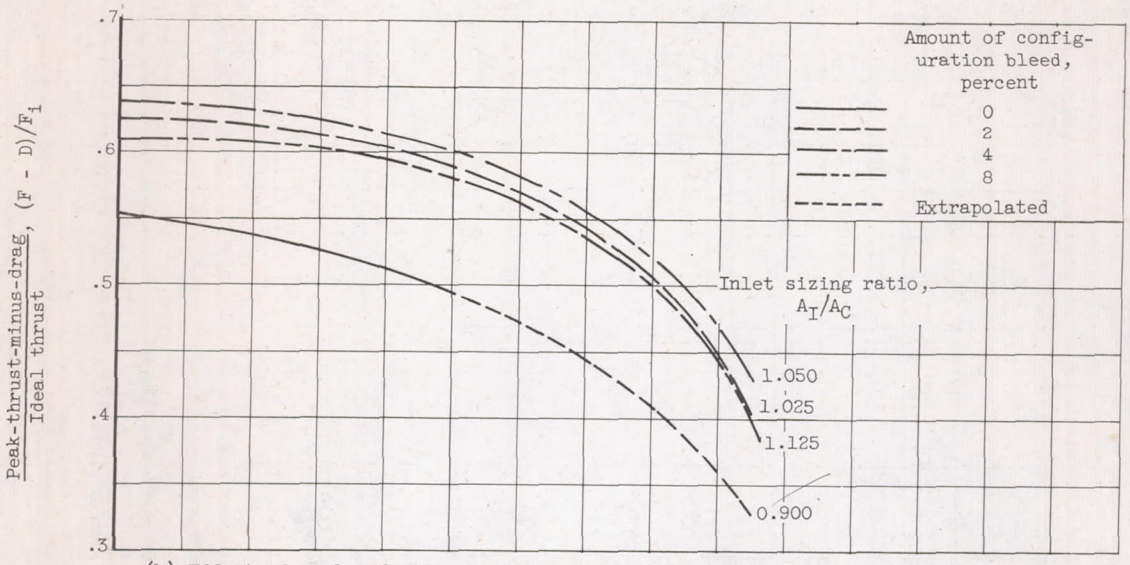

(b) Effect of angle of attack with inlet sized for maximum thrust-minus-drag at zero angle of attack.

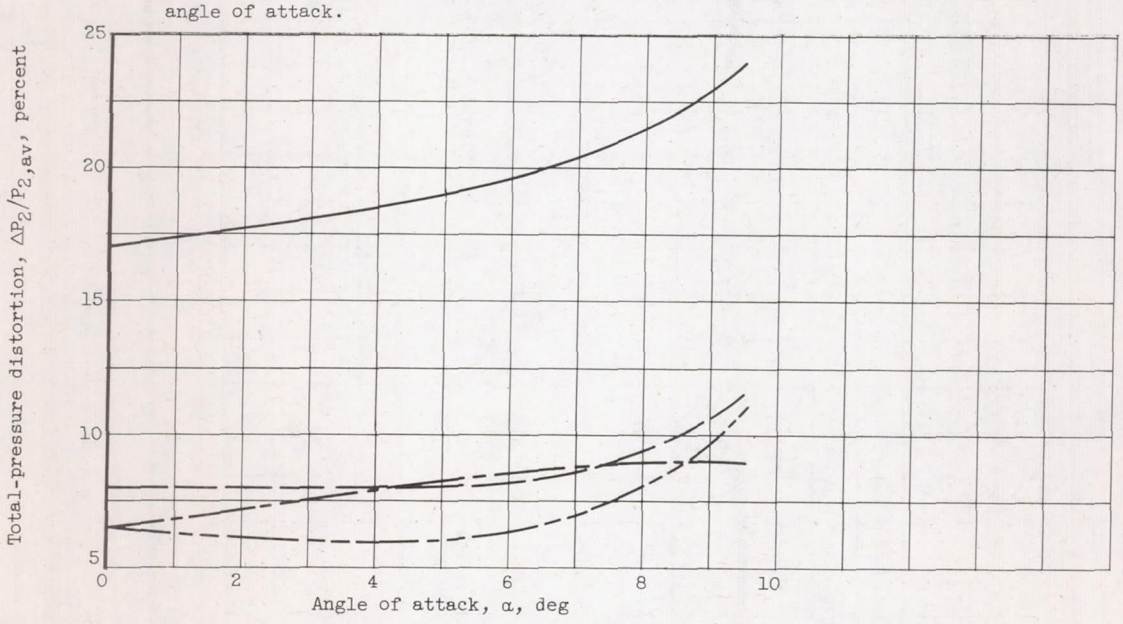

(c) Critical distortion at angle of attack for various bleeds.

Figure 11. - Concluded. Performance summary of bleed configurations at free-stream Mach number of 2.0.

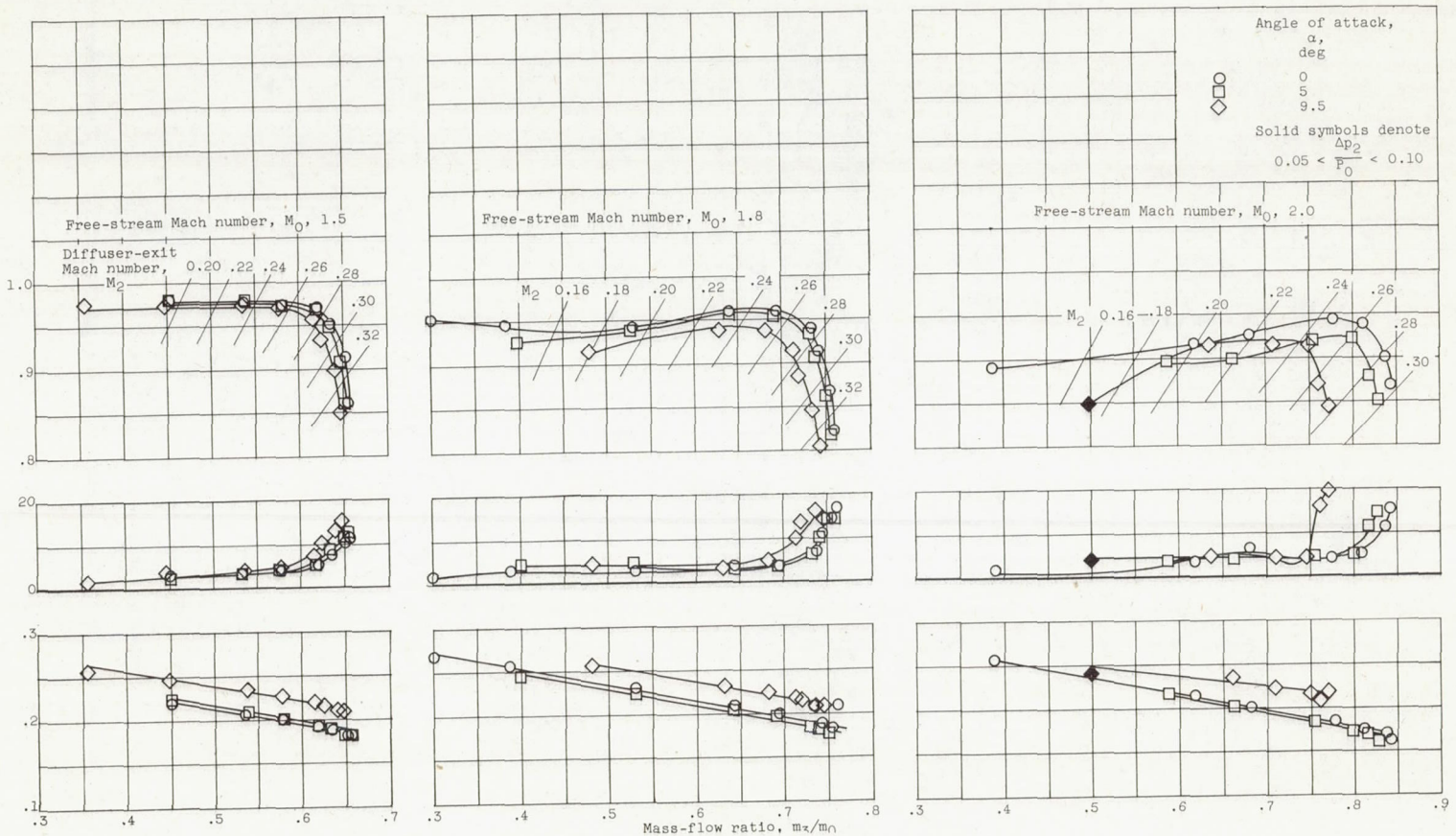

(a) Short fences without side fairings.

Figure 12. - Effect of fences on inlet performance with 8-percent bleed.

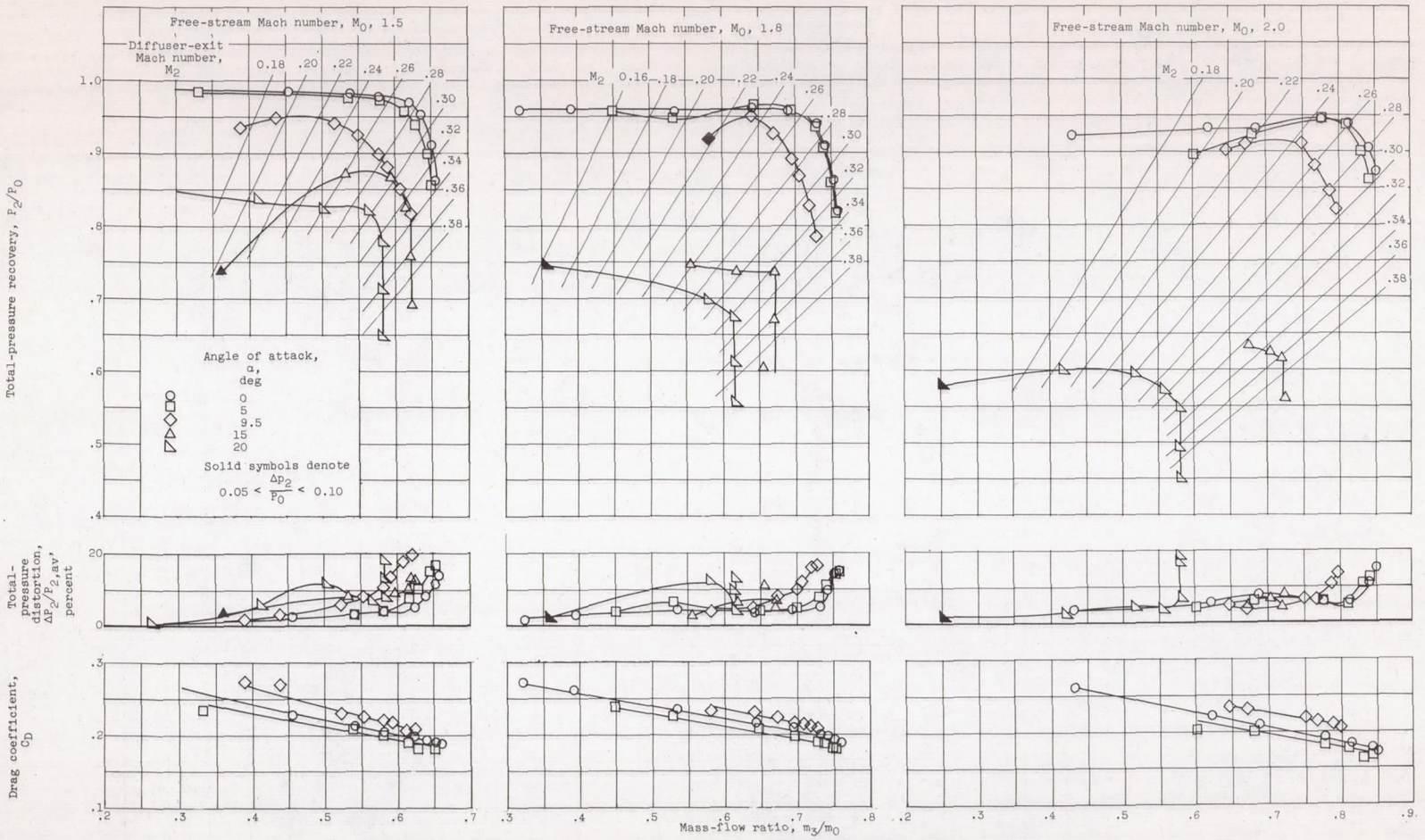

(b) Short fences with side fairings.

Figure 12. - Continued. Effect of fences on inlet performance with 8-percent bleed.

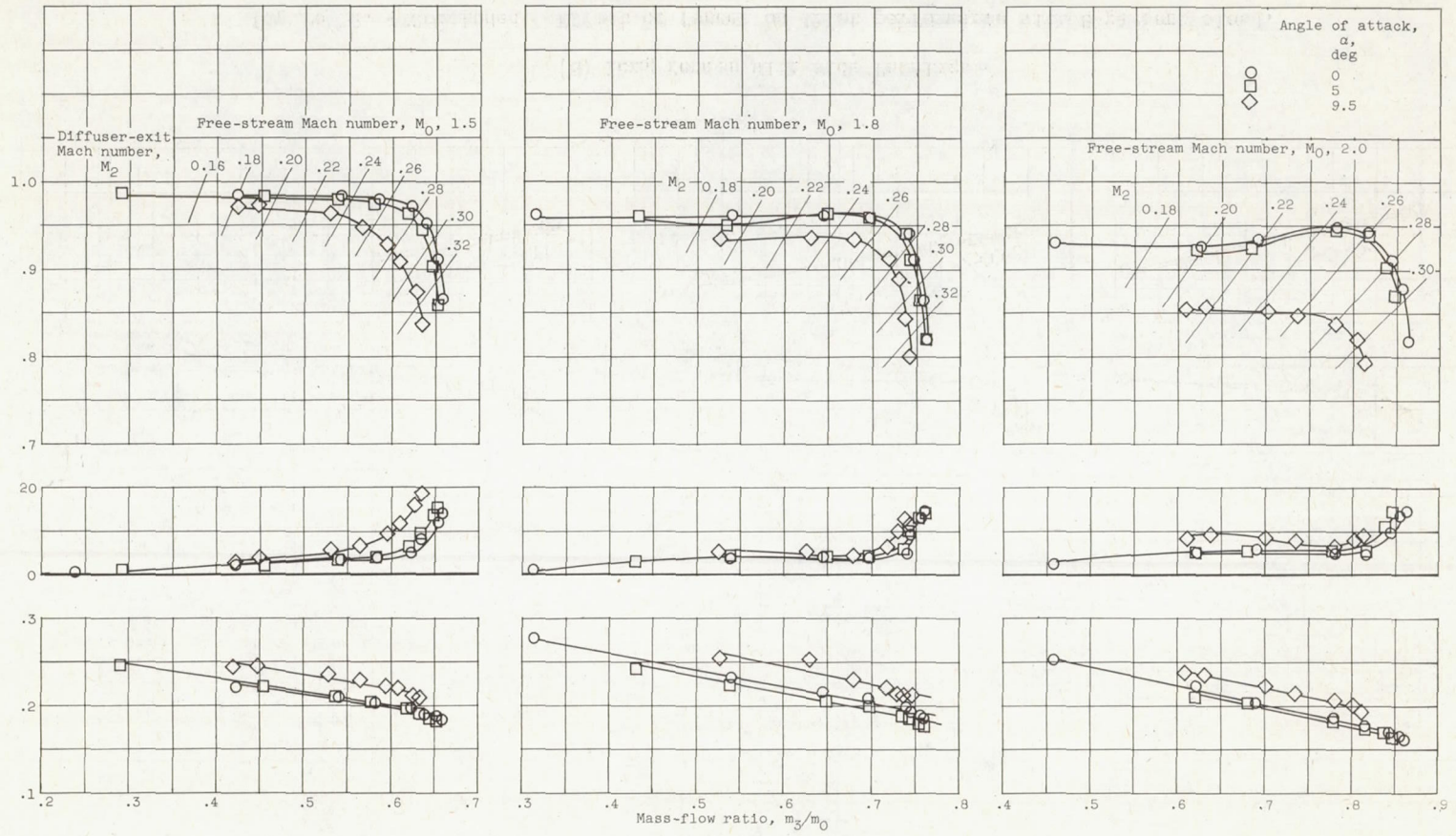

(c) Medium fences with side fairings.

Figure 12. - Continued. Effect of fences on inlet performance with 8-percent bleed.

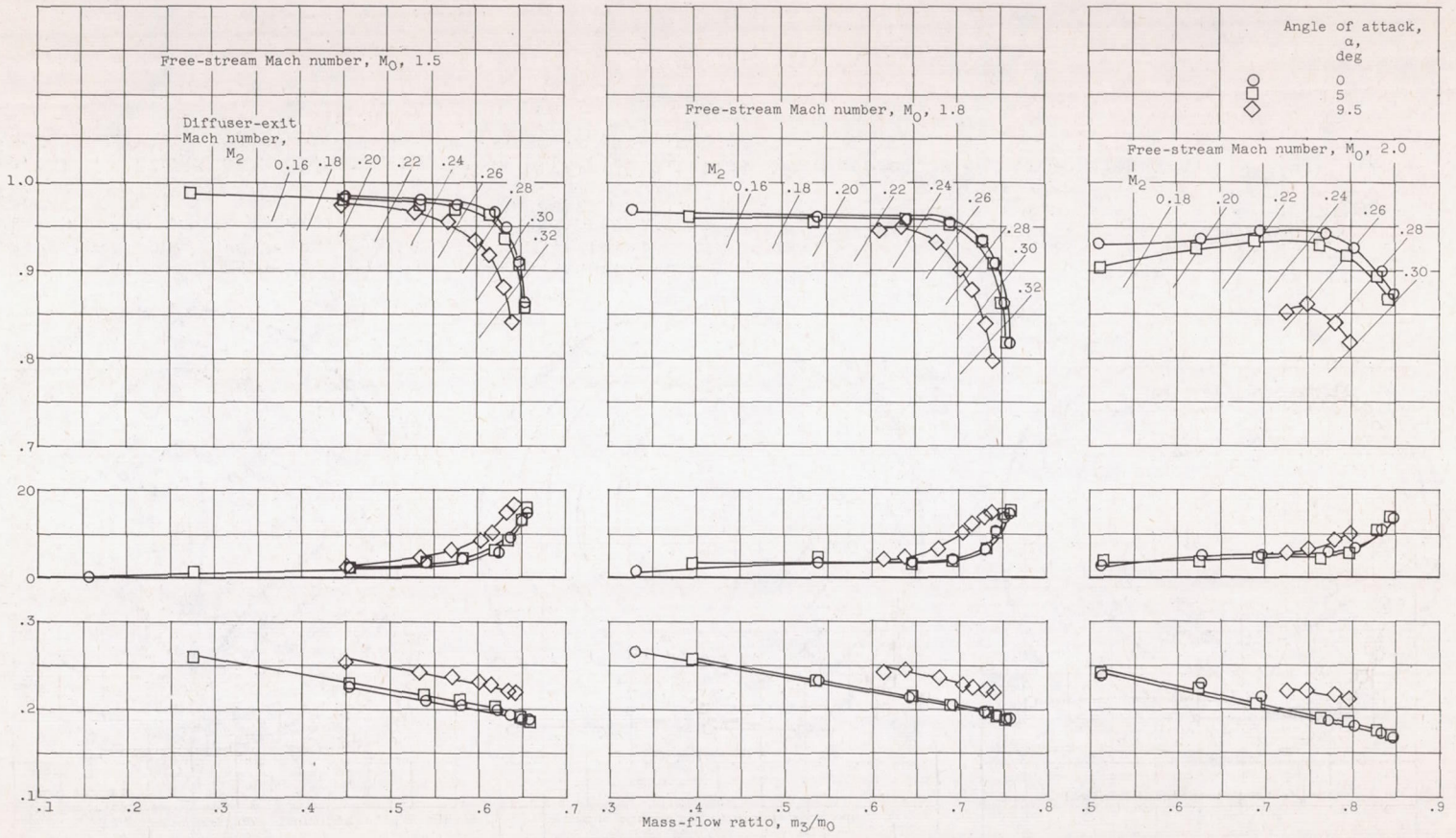

(d) Long fences with side fairings.

Figure 12. - Concluded. Effect of fences on inlet performance with 8-percent bleed.

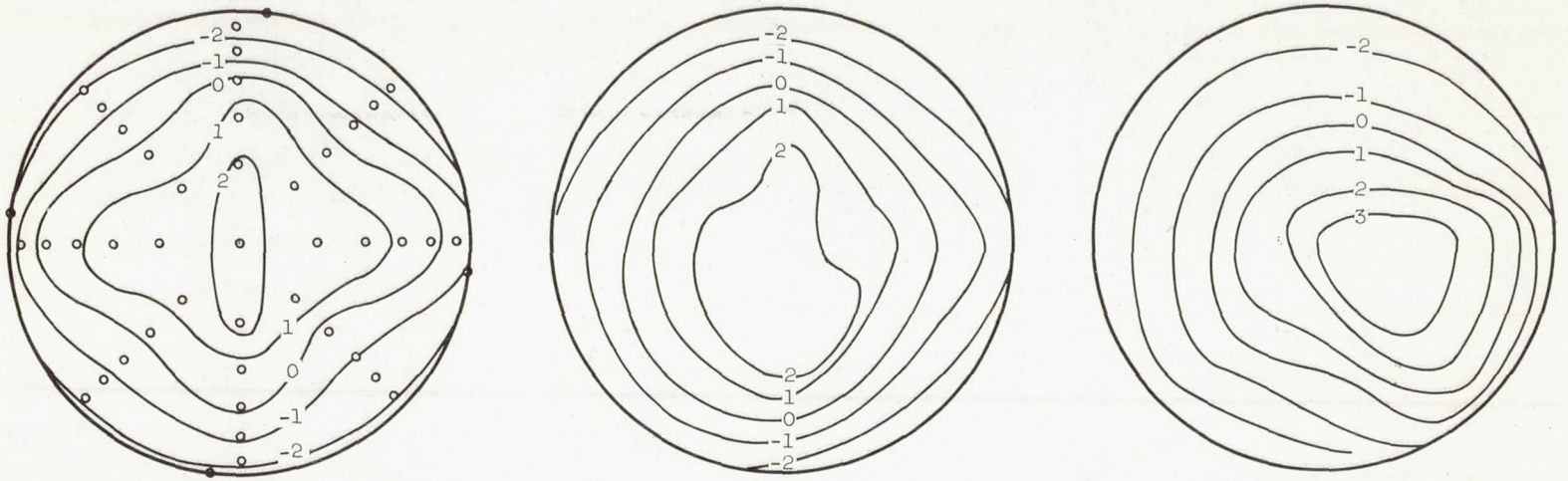

Angle of attack, 0°; mass-flow ratio, 0.817; total-pressure ratio, 0.942; total-pressure distortion, 4.85 percent

Angle of attack, 5°; mass-flow ratio, 0.817; total-pressure ratio, 0.941; total-pressure distortion, 5.48 percent

Angle of attack, 9.5°; mass-flow ratio, 0.781; total-pressure ratio, 0.839; total-pressure distortion, 6.41 percent

Figure 13. - Effect of medium-length fences with side fairings and 8-percent bleed on total-pressure distortion contours at various angles of attack. Free-stream Mach number, 2.0.

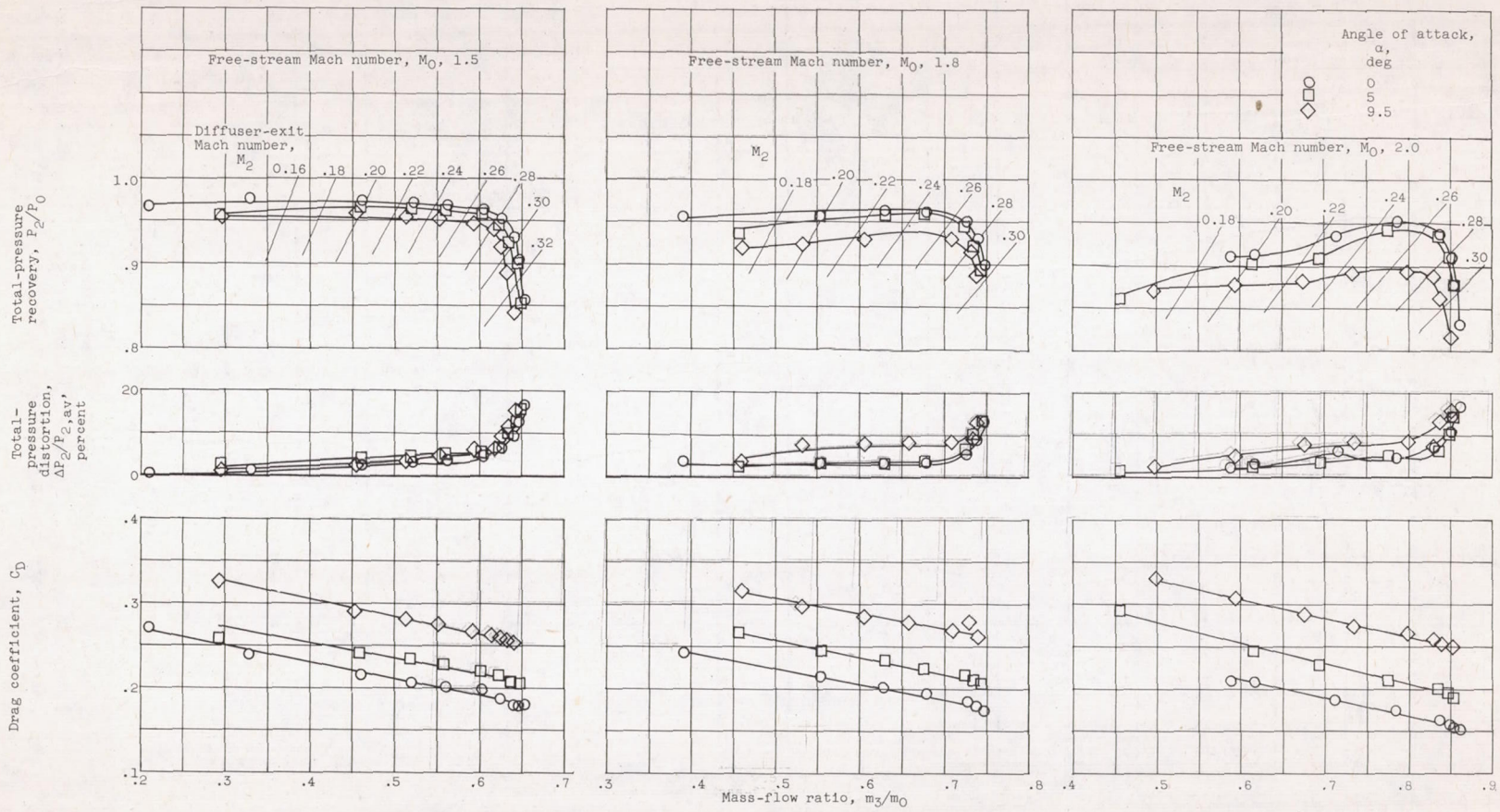

Figure 14. - Performance of bottom inlet with 8-percent bleed and side fairings.

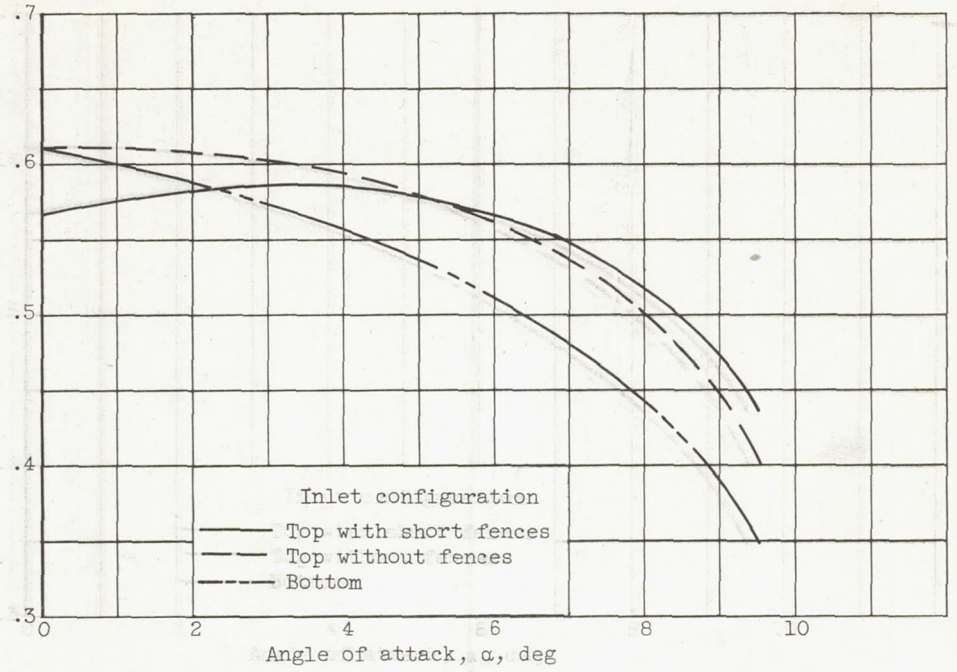

(a) Effect of angle of attack.

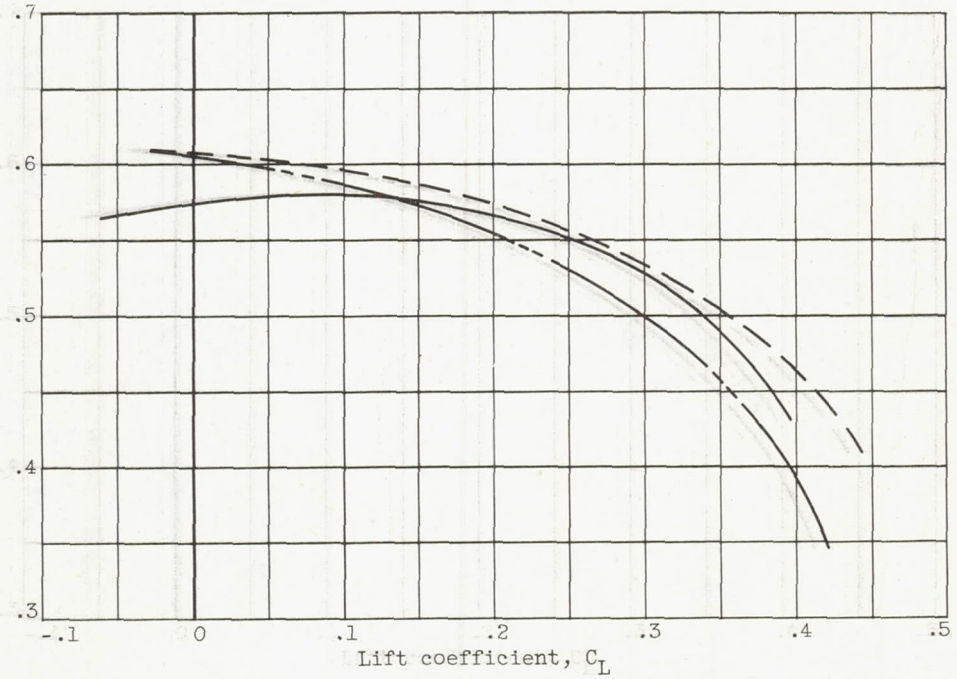

$\frac{\text{Thrust-minus-drag}}{\text{Ideal thrust}}$, $(F - D)/F_i$

(b) Lift-coefficient comparison.

Figure 15. - Comparison of top and bottom inlets with 8-percent bleed and side fairings. Inlets sized for best thrust-minus-drag at zero angle of attack and free-stream Mach number of 2.0.

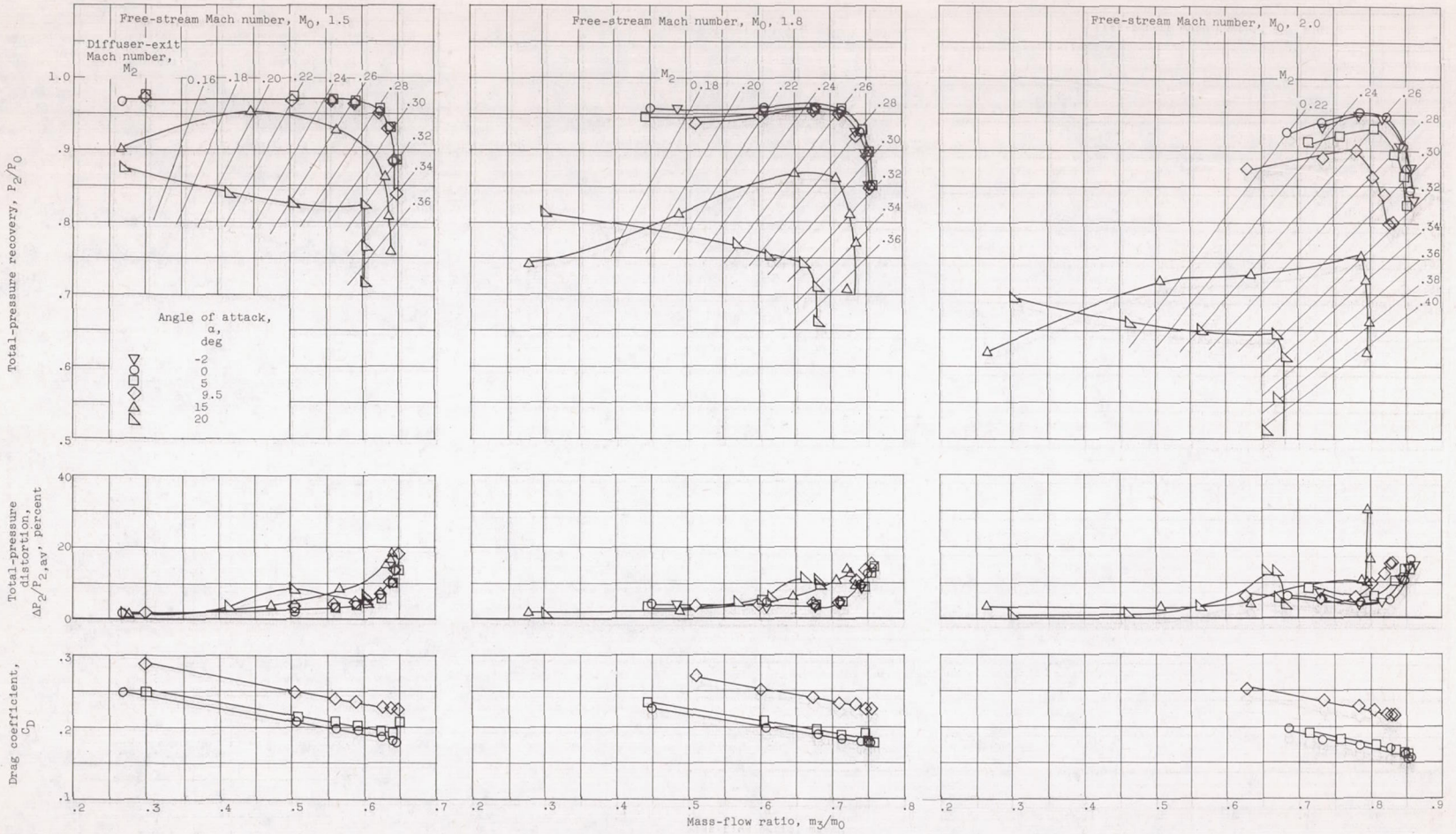

Figure 16. - Effect of round approach on inlet performance with 8-percent bleed and side fairings.

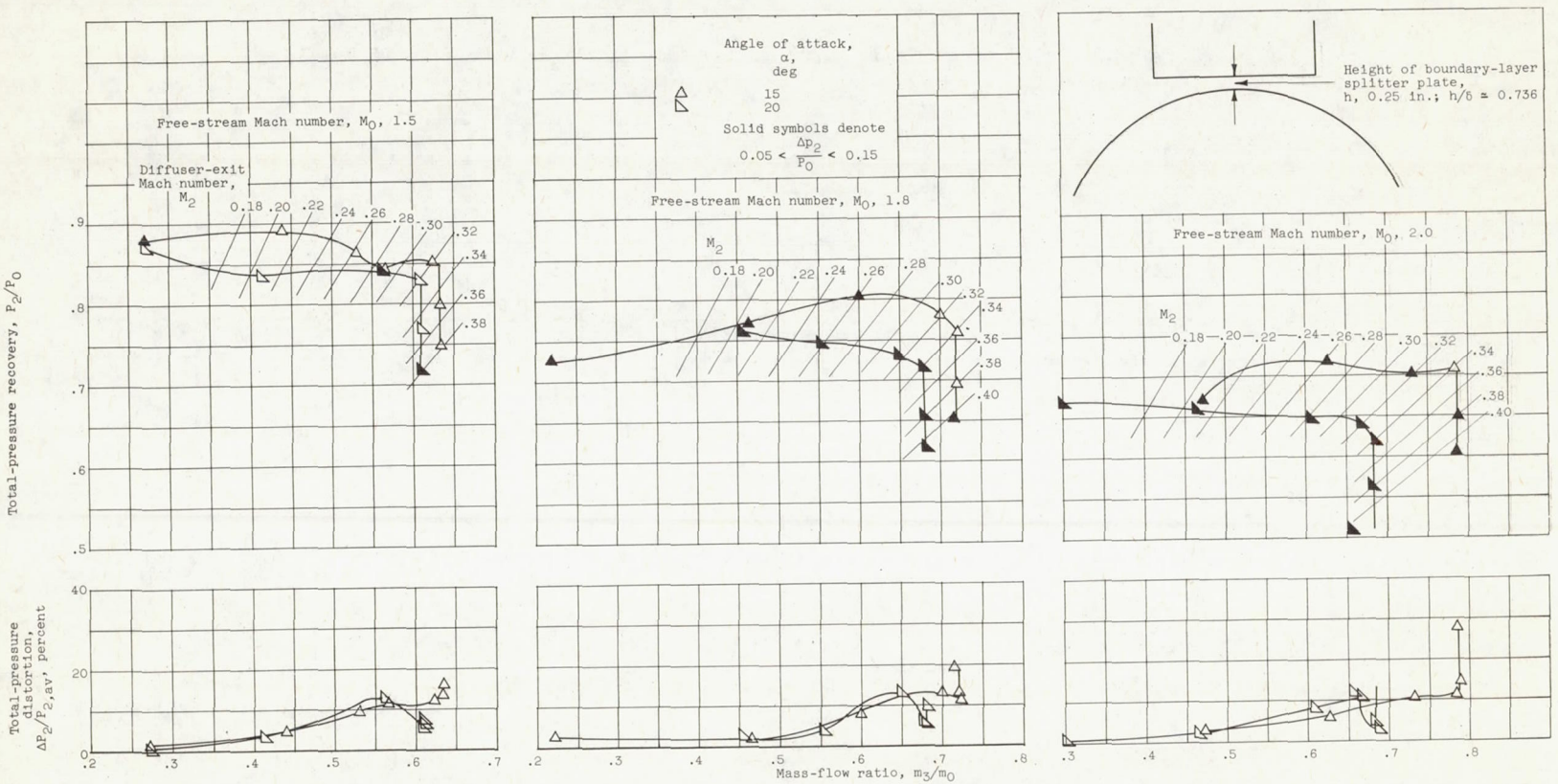

Figure 17. - Reduced h/δ and round approach effects on high angle-of-attack performance with 8-percent bleed and side fairings.

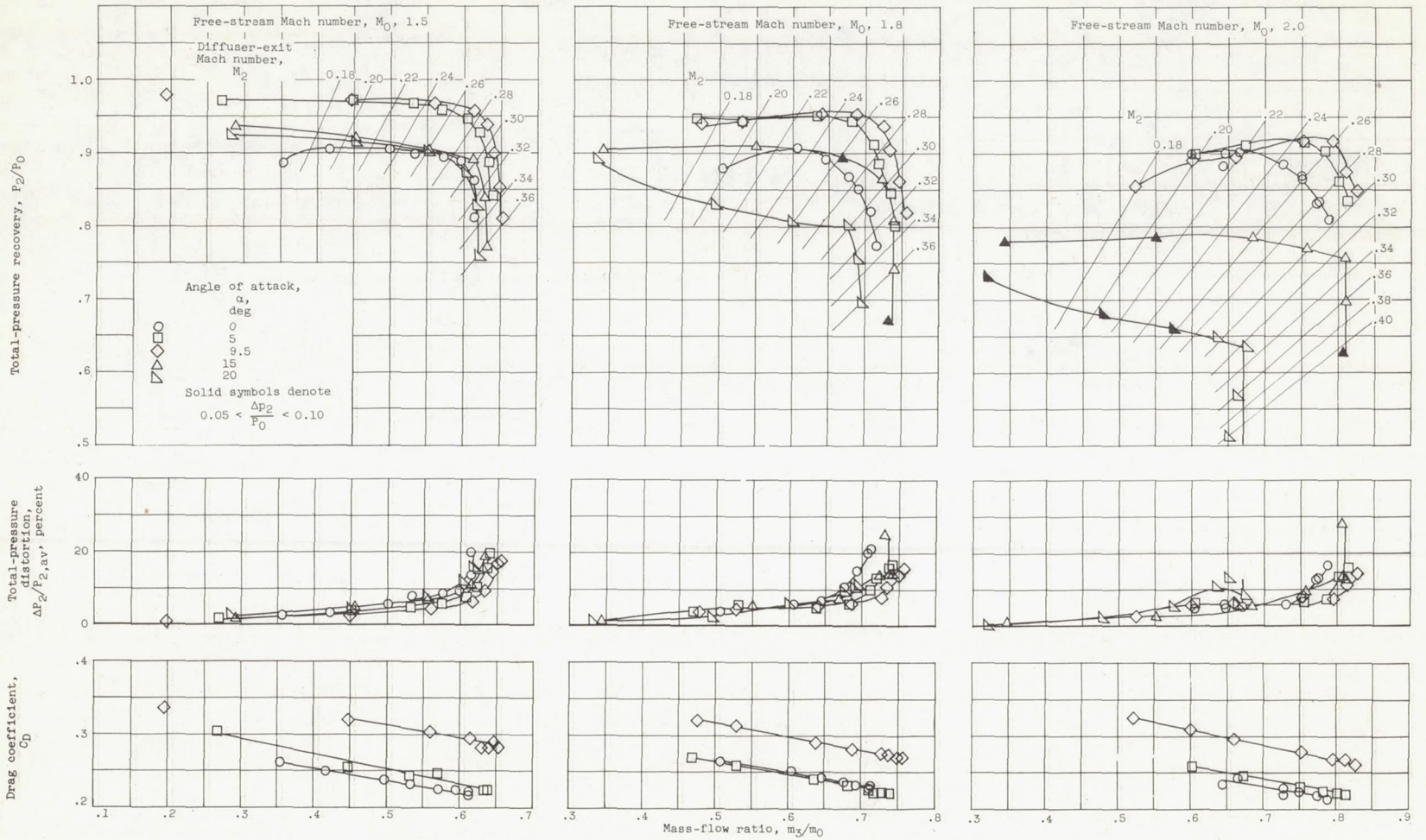

(a) Unfaired canopy with side fairings.

Figure 18. - Inlet performance with canopy and 8-percent bleed.

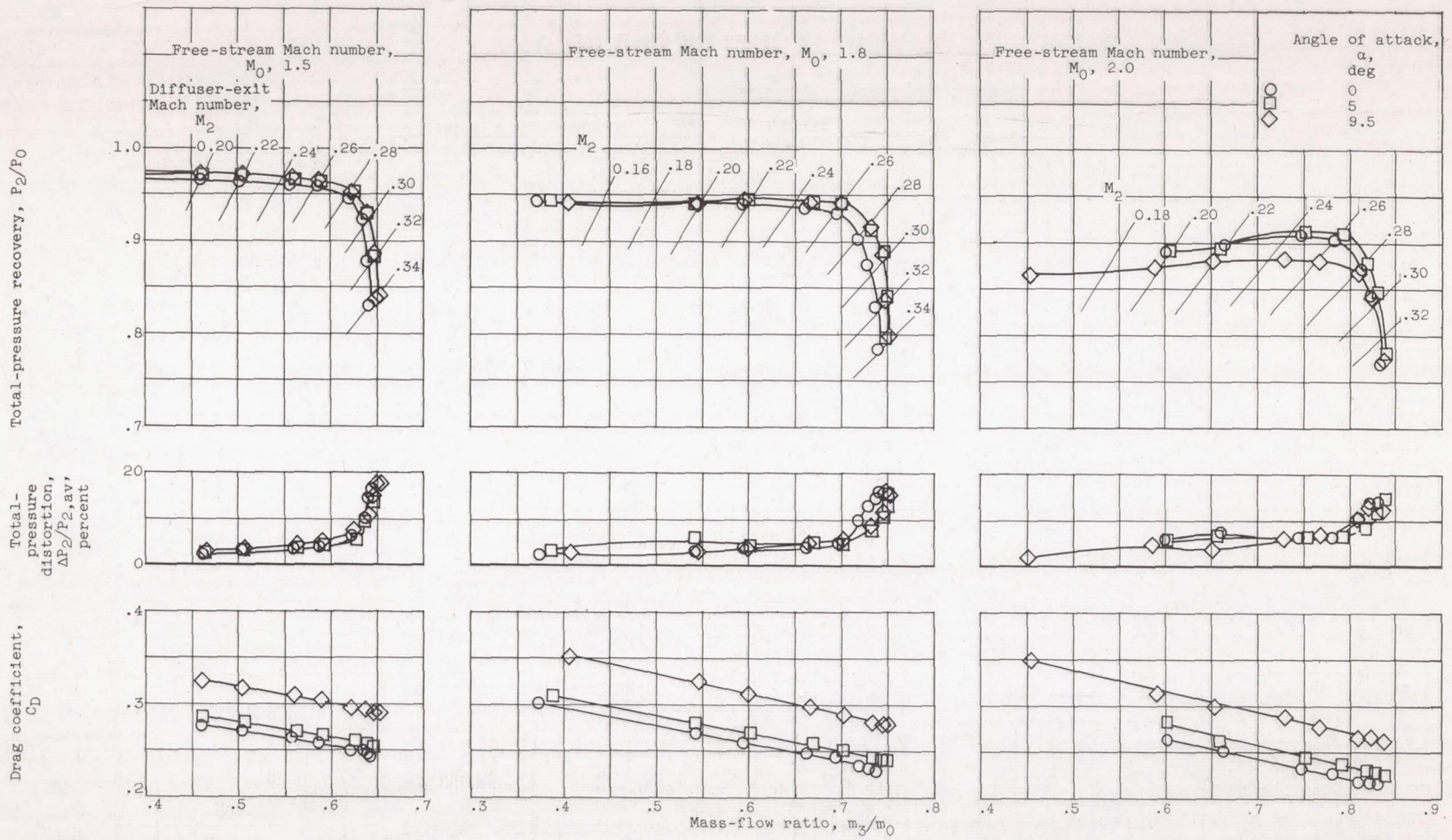

(b) Faired canopy with side fairings.

Figure 18. - Continued. Inlet performance with canopy and 8-percent bleed.

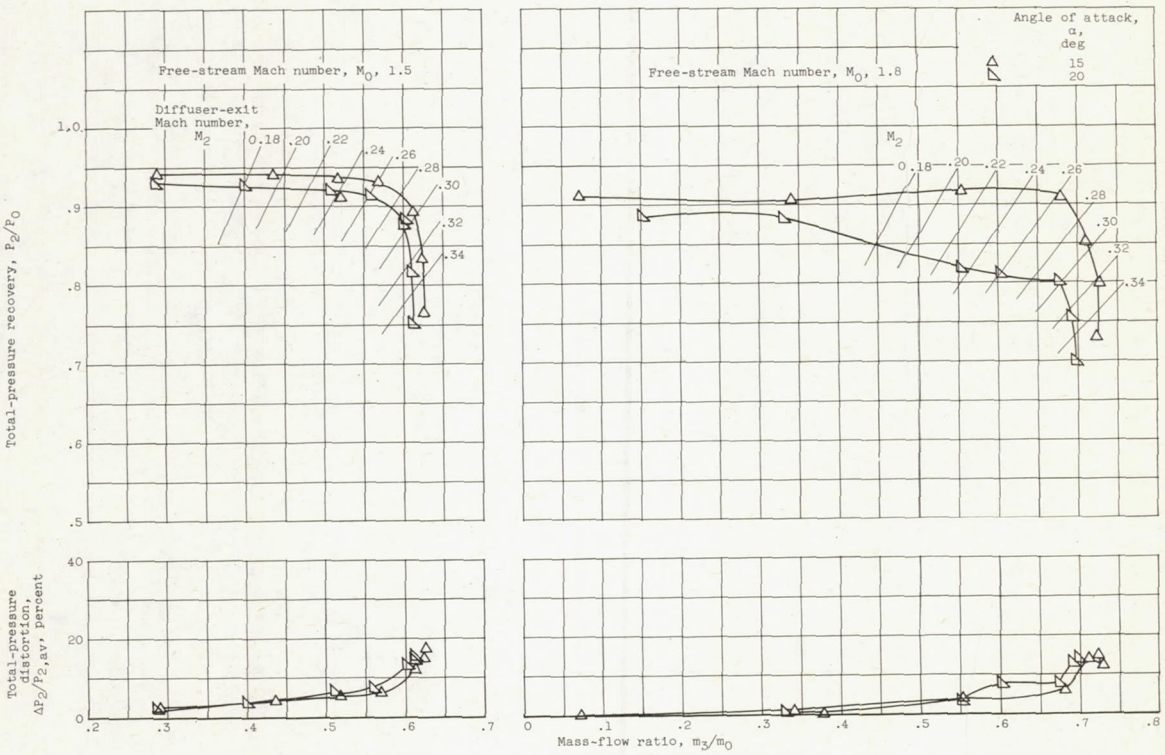

(c) Unfaired canopy without side fairings.

Figure 18. - Continued. Inlet performance with canopy and 8-percent bleed.

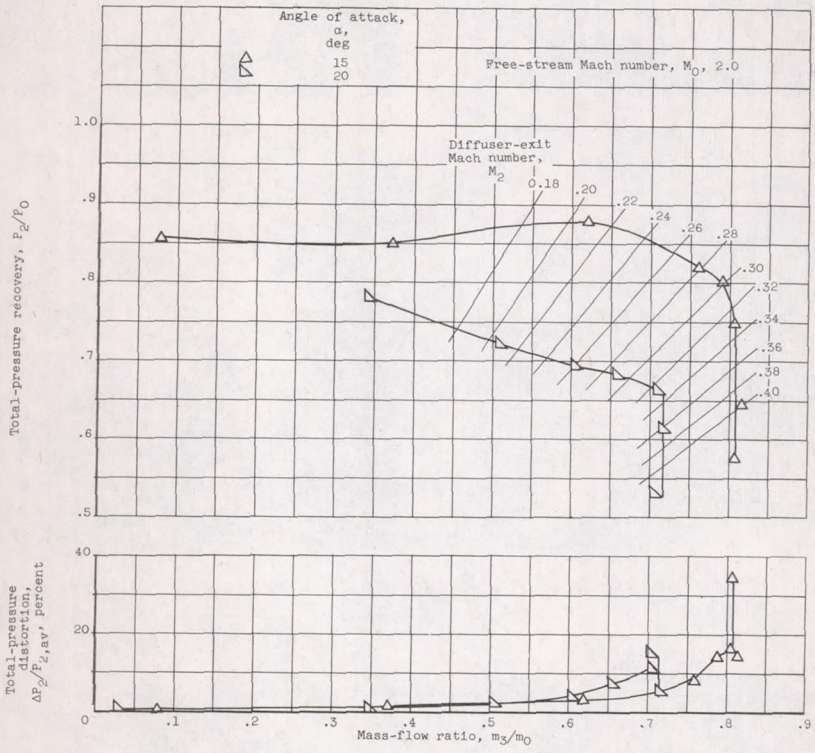

(c) Concluded. Unfaired canopy without side fairings.

Figure 18. - Concluded. Inlet performance with canopy and 8-percent bleed.

Unfaired canopy

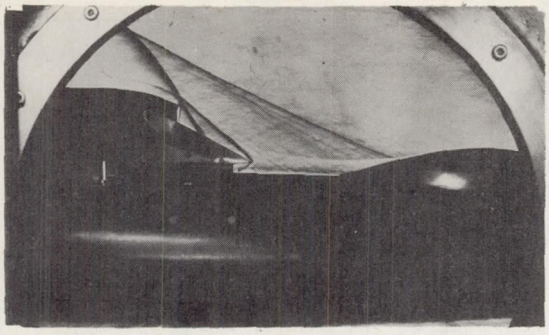

Mass-flow ratio, 0.750; total-pressure ratio, 0.866; diffuser-exit Mach number, 0.26; angle of attack, 0°

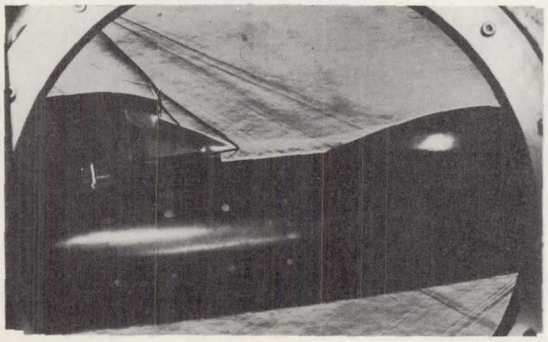

Mass-flow ratio, 0.603; total-pressure ratio, 0.898; diffuser-exit Mach number, 0.201; angle of attack, 5°

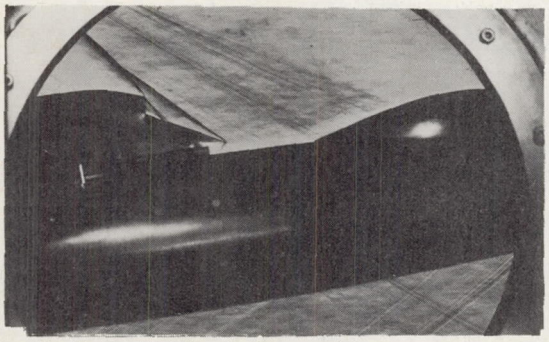

Mass-flow ratio, 0.752; total-pressure ratio, 0.917; diffuser-exit Mach number, 0.245; angle of attack, 9.5°

Faired canopy

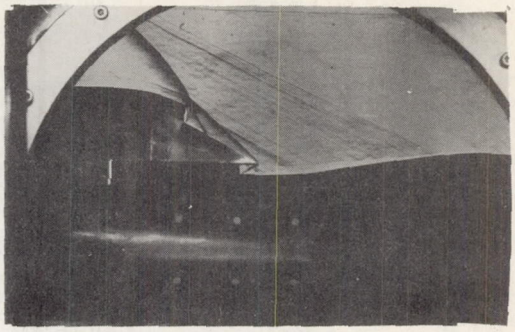

Mass-flow ratio, 0.783; total-pressure ratio, 0.904; diffuser-exit Mach number, 0.26; angle of attack, 0°

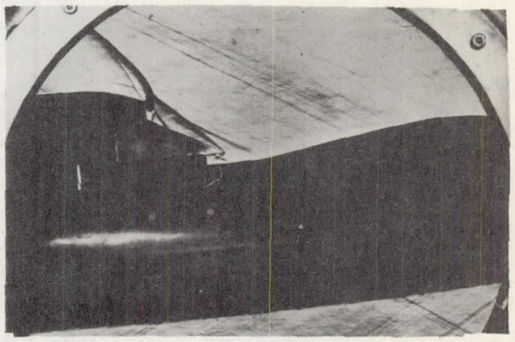

Mass-flow ratio, 0.603; total-pressure ratio, 0.891; diffuser-exit Mach number 0.201; angle of attack, 5°

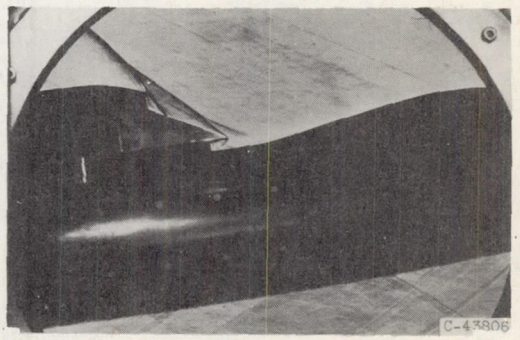

Mass-flow ratio, 0.729; total-pressure ratio, 0.882 diffuser-exit Mach number, 0.245; angle of attack, 9.5°

Figure 19. - Schlieren photographs comparing faired and unfaired canopies at varying angles of attack. Free-stream Mach number, 2.0.

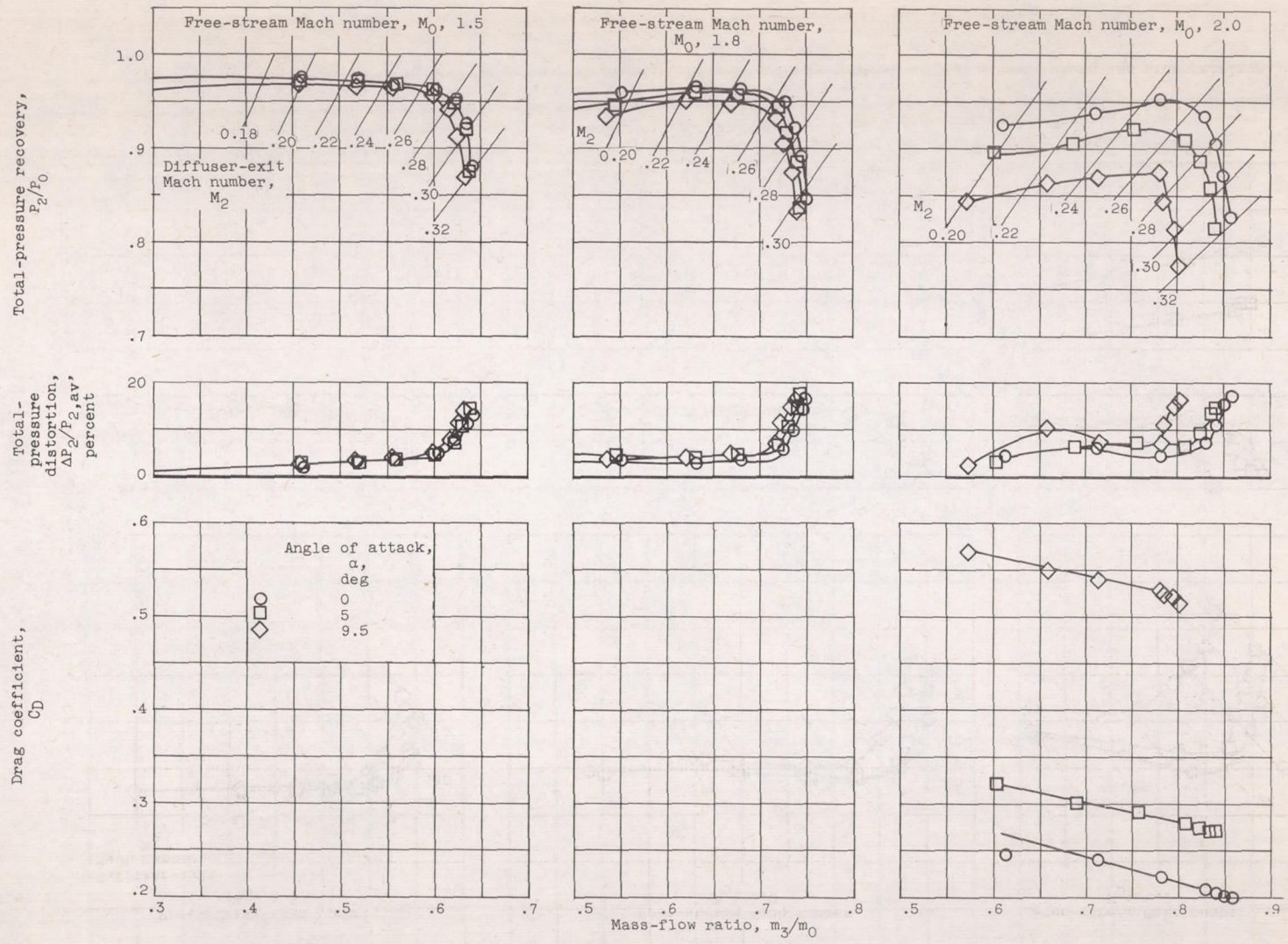

(a) Wings in forward position.

Figure 20. - Effect of simulated 60° delta wing on inlet performance with 8-percent bleed and side fairings.

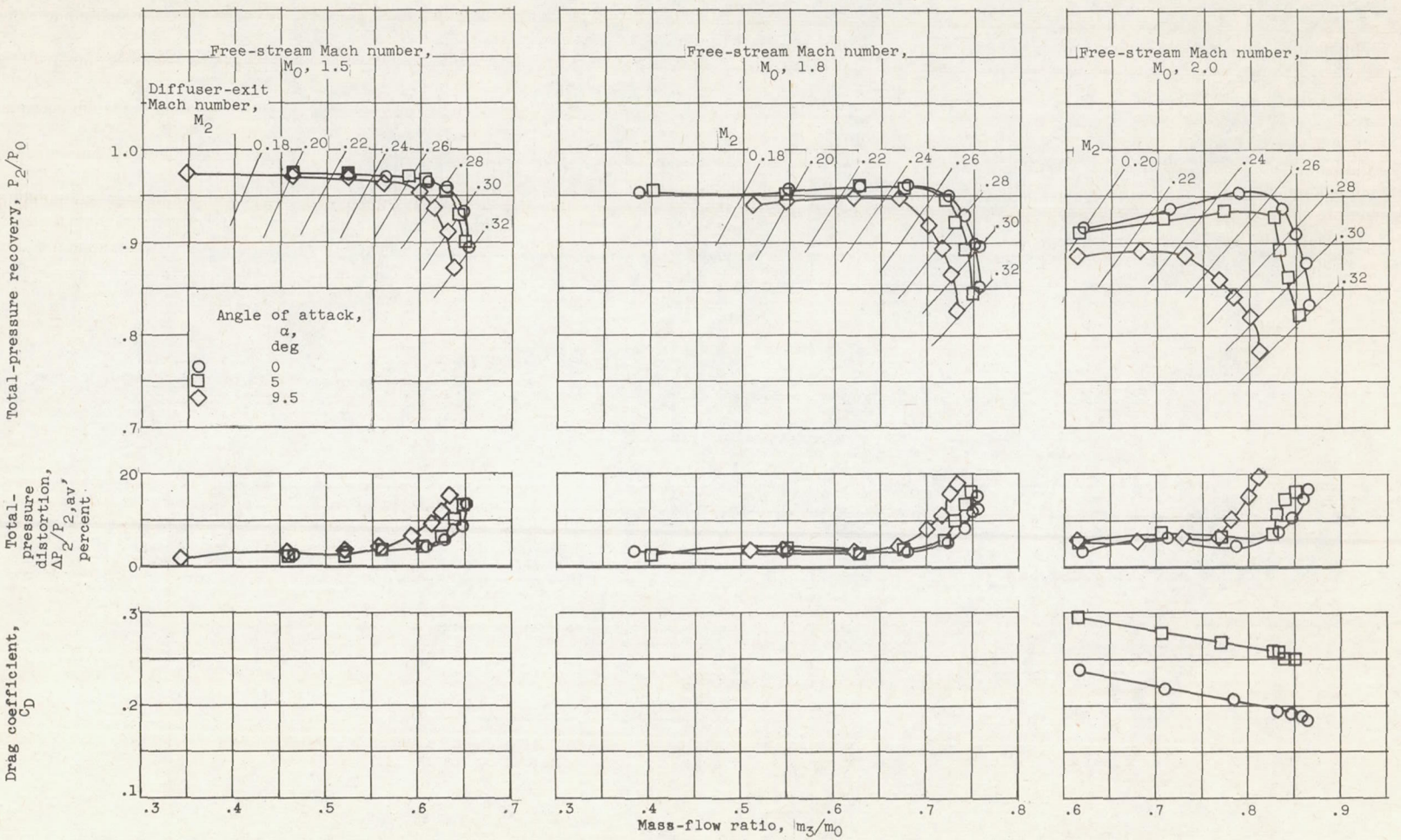

(b) Wings in aft position.

Figure 20. - Concluded. Effect of simulated 60° delta wing on inlet performance with 8-percent bleed and side fairings.

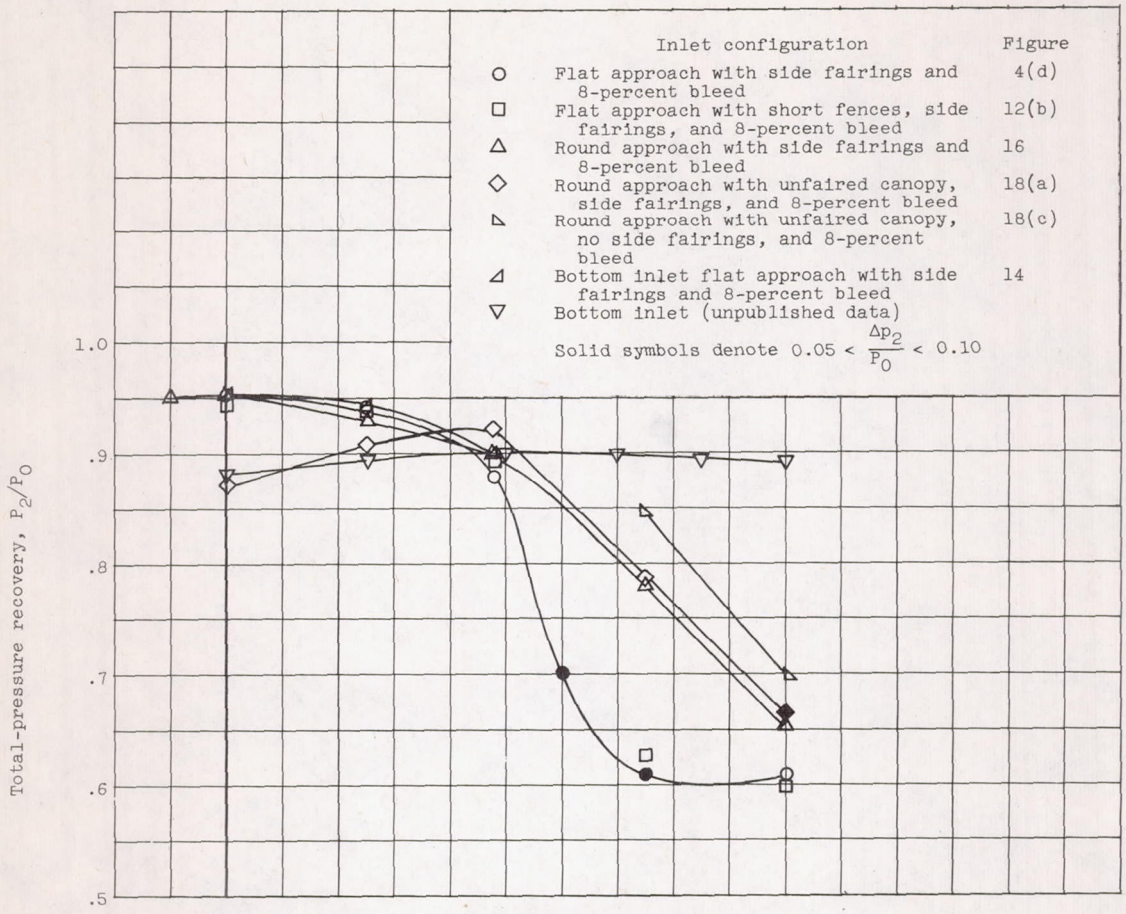

(a) Pressure recovery.

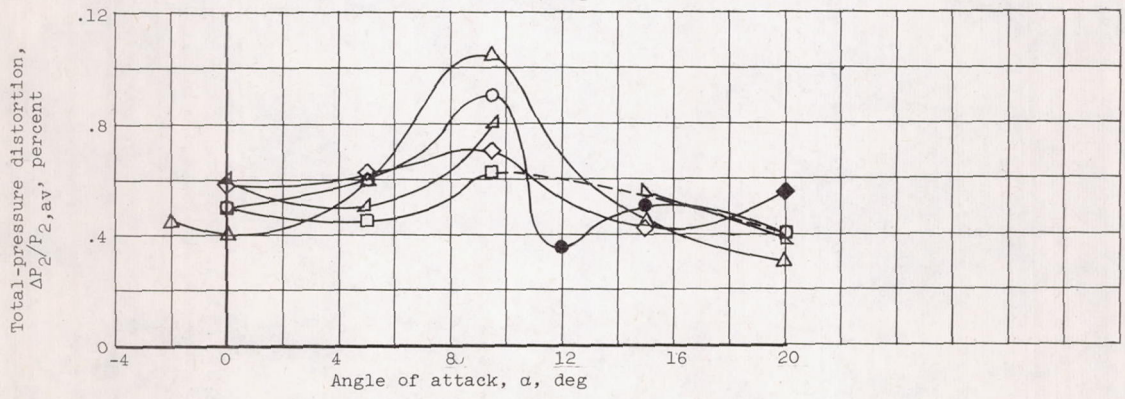

(b) Pressure distortion.

Figure 21. - Angle-of-attack summary of pressure recovery and distortion along constant Mach number line occurring at maximum thrust-minus-drag at zero angle of attack.